




2018

# Investigating Molecular Mechanisms Underlying Mild Phenotype In Friedreich Ataxia Patients With G130v Missense Mutation

Elisia Clark

University of Pennsylvania, [elisiamclark@gmail.com](mailto:elisiamclark@gmail.com)

Follow this and additional works at: <https://repository.upenn.edu/edissertations>

 Part of the [Molecular Biology Commons](#), [Neuroscience and Neurobiology Commons](#), and the [Pharmacology Commons](#)

---

## Recommended Citation

Clark, Elisia, "Investigating Molecular Mechanisms Underlying Mild Phenotype In Friedreich Ataxia Patients With G130v Missense Mutation" (2018). *Publicly Accessible Penn Dissertations*. 2964.  
<https://repository.upenn.edu/edissertations/2964>

This paper is posted at ScholarlyCommons. <https://repository.upenn.edu/edissertations/2964>  
For more information, please contact [repository@pobox.upenn.edu](mailto:repository@pobox.upenn.edu).

---

# Investigating Molecular Mechanisms Underlying Mild Phenotype In Friedreich Ataxia Patients With G130v Missense Mutation

## **Abstract**

Friedreich's Ataxia (FRDA) is an incurable neurodegenerative disease caused by mutations in the frataxin (FXN) gene, resulting in decreased expression of the mitochondrial protein FXN. 2-3% of FRDA patients carry a GAA expansion on one FXN allele, and a missense mutation on the other. The mechanism behind the disease-causing features remains elusive. The phenotype associated with patients carrying point mutations cannot be predicted with certainty; these patients can have a mild or severe clinical outcome, creating a unique platform to understand clinical heterogeneity. FXN is important for proper mitochondrial function, and is involved in Fe-S cluster biogenesis, metabolism, and ATP production. Defining how missense mutations influence FXN's processing and role in energy production and cellular metabolism will help identify pathways that are affected during disease progression, begin to explain the varying phenotypes, and establish a biochemical genotype-phenotype correlation. Of all disease-associated mutations, patients carrying the G130V missense mutation are of most interest because they have less than 5 % of control mature FXN levels but evolve to a milder phenotype with slower disease progression and significantly lower occurrence of cardiomyopathy, scoliosis, and diabetes. In this thesis, I identified impaired protein processing from FXN42-210 to FXN81-210 as the mechanism by which FXN missense mutations result in lower mature FXN81-210 levels in mutation-selective ways by overexpression studies and subcellular fractionation. This was also true for a novel FXN W168R missense mutation associated with severely low FXN levels and phenotype. Multiple features of mitochondrial dysfunction associated with severe phenotype in typical FRDA, and compared them to G130V patients were also assessed in order to understand the molecular mechanisms underlying the milder phenotype. Fibroblasts from G130V patients have increased mitochondrial ferritin immunoreactivity by immunocytochemistry, increased mitochondrial aconitase activity measured by enzymatic conversion of citrate to isocitrate, and increased Krebs cycle metabolic activity measured by LC-MS isotopologue tracer studies, compared to typical FRDA fibroblasts. Overall, fibroblasts from G130V patients appear to have improved mitochondrial function compared to typical FRDA patients, thus providing a rationale linking G130V functional capacity with milder phenotype.

## **Degree Type**

Dissertation

## **Degree Name**

Doctor of Philosophy (PhD)

## **Graduate Group**

Pharmacology

## **First Advisor**

David Lynch

## **Second Advisor**

Kelly Jordan-Sciutto

---

**Keywords**

frataxin, Friedreich ataxia, missense mutation

**Subject Categories**

Molecular Biology | Neuroscience and Neurobiology | Pharmacology

INVESTIGATING MOLECULAR MECHANISMS UNDERLYING MILD PHENOTYPE IN  
FRIEDREICH ATAXIA PATIENTS WITH G130V MISSENSE MUTATION

Elisia Clark

A DISSERTATION

in

Pharmacology

Presented to the Faculties of the University of Pennsylvania

in

Partial Fulfillment of the Requirements for the

Degree of Doctor of Philosophy

2018

Supervisor of Dissertation

---

Dr. David R. Lynch MD, PhD, Professor of Neurology

Graduate Group Chairperson

---

Dr. Julie A. Blendy, PhD, Professor of Pharmacology

Dissertation Committee

Dr. Kelly Jordan-Sciutto, PhD, Professor of Pharmacology

Dr. Edward (Jim) Delikatny, PhD, Professor of Radiology

Dr. Steven Thomas MD, PhD, Professor of Pharmacology

Dr. Robert Wilson, MD, PhD, Professor of Pathology and Laboratory Medicine

INVESTIGATING MOLECULAR MECHANISMS UNDERLYING MILD PHENOTYPE IN  
FRIEDREICH ATAXIA PATIENTS WITH G130V MISSENSE MUTATION

COPYRIGHT

2018

ELISIA MONIQUE CLARK

This work is licensed under the  
Creative Commons Attribution-  
NonCommercial-ShareAlike 3.0  
License

To view a copy of this license, visit

<https://creativecommons.org/licenses/by-nc-sa/3.0/us/>

## DEDICATION

I would like to dedicate this thesis to my parents who worked diligently to support me in accomplishing this milestone. You have truly impacted my research in ways you cannot imagine.

I would also like to dedicate this thesis to Dr. Jessica Panzer MD, PhD, who taught me every technique and scientific skill that has allowed me to be the researcher I am today. Her mentorship and her life has impacted and inspired me in many ways, and for that I am forever grateful.

## ACKNOWLEDGEMENTS

I would first like to acknowledge my thesis advisor, Dr. David Lynch, for his guidance during my time in the lab. I am most thankful for his mentorship, support, flexibility, and quick response time. I am also thankful for his direction and the freedom to pursue research questions that were of interest to me. I would also like to thank the current members of the lab Hong Lin, Ying Dong, Amy Salovin, Nathan Warren, and Joseph Johnson for their support, feedback and listening ears. And I am thankful to my thesis committee Dr. Kelly Jordan-Sciutto, Dr. Edward (Jim) Delikatny, Dr. Steven Thomas, and Dr. Robert Wilson for their support, encouragement, and words of wisdom regarding my research, career, and life.

I would like to specially thank the Friedreich ataxia patients and members of the community who volunteered and provided samples for studies as part of this thesis, and the Friedreich ataxia Research Alliance for their commitment to aligning scientists, patients, clinicians, government agencies, pharmaceutical companies and other organizations dedicated to curing Friedreich ataxia. I would also like to thank the Lynch clinical team Lauren Hauser, Cassandra Strawser, Kimberly Schadt, Mckenzie Wells, and Maya Patel for coordinating and collecting patients samples.

I wish to acknowledge my collaborators Drs. Jill and Marek Napierala of University of Alabama for their work with the primary patient fibroblasts and frataxin quantification, Drs. Clementina Mesaros and Andrew Worth for their help with the isotope labeling studies and data analysis, Dr. Joshua Jackson for help with live imaging, and the Intellectual and Developmental Disabilities Research Center for training on confocal microscopy.

I would also like to thank the Pharmacology Graduate Group and the current chair Dr. Julie Blendy and coordinator Sarah Squire for their support throughout my time as a graduate student, and the Solomon and Catherine Erulkar Traveling Fellowship for awarding me an opportunity to present my research at the International Ataxia Research Conference in Pisa, Italy.

I would also like to acknowledge the National Institutes of Health (NIH), Friedreich ataxia Research Alliance (FARA), and Friedreich ataxia Center for Excellence (COE) for funding to make this research possible.

Last but not least, I would like to thank my classmates, family, and friends for their support and encouragement.



## ABSTRACT

### INVESTIGATING MOLECULAR MECHANISMS UNDERLYING MILD PHENOTYPE IN FRIEDREICH ATAXIA PATIENTS WITH G130V MISSENSE MUTATION

Elisia M. Clark

David R. Lynch MD, PhD

Friedreich's Ataxia (FRDA) is an incurable neurodegenerative disease caused by mutations in the frataxin (*FXN*) gene, resulting in decreased expression of the mitochondrial protein FXN. 2-3% of FRDA patients carry a GAA expansion on one FXN allele, and a missense mutation on the other. The mechanism behind the disease-causing features remains elusive. The phenotype associated with patients carrying point mutations cannot be predicted with certainty; these patients can have a mild or severe clinical outcome, creating a unique platform to understand clinical heterogeneity. FXN is important for proper mitochondrial function, and is involved in Fe-S cluster biogenesis, metabolism, and ATP production. Defining how missense mutations influence FXN's processing and role in energy production and cellular metabolism will help identify pathways that are affected during disease progression, begin to explain the varying phenotypes, and establish a biochemical genotype-phenotype correlation. Of all disease-associated mutations, patients carrying the G130V missense mutation are of most interest because they have less than 5 % of control mature FXN levels but evolve to a milder phenotype with slower disease progression and significantly lower occurrence of cardiomyopathy, scoliosis, and diabetes. In this

thesis, I identified impaired protein processing from FXN<sup>42-210</sup> to FXN<sup>81-210</sup> as the mechanism by which FXN missense mutations result in lower mature FXN<sup>81-210</sup> levels in mutation-selective ways by overexpression studies and subcellular fractionation. This was also true for a novel FXN W168R missense mutation associated with severely low FXN levels and phenotype. Multiple features of mitochondrial dysfunction associated with severe phenotype in typical FRDA, and compared them to G130V patients were also assessed in order to understand the molecular mechanisms underlying the milder phenotype. Fibroblasts from G130V patients have increased mitochondrial ferritin immunoreactivity by immunocytochemistry, increased mitochondrial aconitase activity measured by enzymatic conversion of citrate to isocitrate, and increased Krebs cycle metabolic activity measured by LC-MS isotopologue tracer studies, compared to typical FRDA fibroblasts. Overall, fibroblasts from G130V patients appear to have improved mitochondrial function compared to typical FRDA patients, thus providing a rationale linking G130V functional capacity with milder phenotype.

## TABLE OF CONTENTS

DEDICATION .....	III
ABSTRACT .....	VI
TABLE OF CONTENTS .....	VIII
LIST OF TABLES .....	IX
LIST OF FIGURES .....	X
ABBREVIATIONS .....	XII
CHAPTER 1: INTRODUCTION TO FRIEDREICH ATAXIA.....	1
CHAPTER 2: SELECTED MISSENSE MUTATIONS IMPAIR FXN PROCESSING .....	10
CHAPTER 3: IDENTIFICATION OF A NOVEL MISSENSE MUTATION- FXN <sup>W168R</sup> .....	32
CHAPTER 4: G130V ALLEVIATES MITOCHONDRIA DYSFUNCTION .....	46
CHAPTER 5: CONCLUSIONS AND FUTURE DIRECTIONS .....	65
REFERENCES.....	74

## LIST OF TABLES

Table 2.1 Clinical measures comparing FRDA homozygous and heterozygous patients.....	45
Table 2.2 Clinical measures comparing FXNG130V and FXNI154F patients with other FRDA heterozygous patients.....	46

## LIST OF FIGURES

Figure 2.1 Selected FRDA-associated missense mutations decrease FXN <sup>81-210</sup> levels.....	39
Figure 2.2 Selected FRDA-associated missense mutations do not impair FXN association with mitochondria.....	40
Figure 2.3 Selected FRDA-associated missense mutations impair processing from FXN <sup>42-210</sup> to FXN <sup>81-210</sup> .....	41
Figure 2.4 Missense mutations I154F and G130V enhance the association of FXN <sup>42-210</sup> with MPP.....	42
Figure 2.5 Increasing G130V and I154F FXN <sup>1-210</sup> levels does not increase FXN <sup>81-210</sup> levels.....	43
Figure 2.6 Impaired FXN processing from FXN <sup>42-210</sup> to FXN <sup>81-210</sup> occurs in fibroblasts from FRDA patients with G130V.....	44
Figure 3.1 W168R decrease FXN <sup>81-210</sup> levels.....	56
Figure 3.2 W168R does not impair FXN association with mitochondria.....	57
Figure 3.3 W168R enhances the association of FXN <sup>42-210</sup> with MPP.....	58
Figure 3.4 W168R impairs processing from FXN <sup>42-210</sup> to FXN <sup>81-210</sup> .....	59
Figure 3.5 Increasing W168R FXN <sup>1-210</sup> levels does not increase FXN <sup>81-210</sup> levels.....	60
Figure 4.1 Decreased mitochondrial ferritin in as absent in G130V patient fibroblasts.....	73
Figure 4.2 Increased Mitochondria Aconitase Activity in G130V FRDA patient fibroblasts.....	74
Figure 4.3 Increased TCA metabolic activity in G130V FRDA patient fibroblasts.....	75
Figure 4.4 G130V Patients have retained mitochondria structure and increased glycogen.....	76
Figure 4.5 Mitochondria fragmentation in FRDA patient fibroblasts.....	77
Figure 4.6 Mitochondria fusion is preserved in G130V patient fibroblasts.....	78

Supplemental Figure 4.2 FXN overexpression reverses mitochondria fragmentation...79

## ABBREVIATIONS

9HPT	9 Hole peg test
ADL	Activities of daily living
ATP	Adenosine triphosphate
BCA	Bicinchoninic acid
BSA	Bovine serum albumin
CNS	Central nervous system
CTRL	Control
CoQ <sub>10</sub>	Coenzyme Q <sub>10</sub>
DNA	Deoxyribonucleic acid
DRG	Dorsal root ganglia
DTT	Dithiothreitol
ECL	Enhanced chemiluminescence
EDTA	Ethylenediaminetetraacetic acid
FARS	Friedreich ataxia rating scale
Fe-S	Iron-Sulfur

FRDA	Friedreich ataxia
FtMt	Mitochondrial Ferritin
FXN	Frataxin
GAA	Guanine-Adenine-Adenine
GAPDH	Glyceraldehyde 3-phosphate dehydrogenase
GFP	Green Fluorescent Protein
HA	Hemagglutinin
HCL	Hydrogen chloride
HDAC	Histone deacetylase
HDACi	Histone deacetylase inhibitor
HEK293	Human embryonic kidney cells
HMZ	Homozygous
HRP	Horseradish peroxidase
HTZ	Heterozygous
ISC	Iron sulfur cluster
IgG	Immunoglobulin
IP	Immunoprecipitation



LC-MS	Liquid Chromatography Mass Spectrometry
MG132	Proteasome inhibitor
MITO	Mitochondria
MPP	Mitochondria processing peptidase
mRNA	Messenger ribonucleic acid
MRI	Magnetic resonance imaging
OXPHOS	Oxidative Phosphorylation
PAGFP	Photoactivatable green florescent protein
PVDF	Polyvinylidene difluoride
RNA	Ribonucleic acid
ROS	Reactive oxygen species
SDS-PAGE	Sodium dodecyl sulfate polyacrylamide gel electrophoresis
SEM	Standard error of the mean
SOD	Superoxide dismutase
T25FW	Timed 25-foot walk
TCA	Tricarboxylic acid
WT	Wild type

Z-score

Performance measure

## **Chapter 1: Introduction to Friedreich ataxia**

### **1.1 Friedreich ataxia Pathogenesis**

Friedreich's Ataxia (FRDA) is an autosomal recessive, neurodegenerative disorder that affects 1 in every 50,000 people in the United States. FRDA was first described in 1863 as a disease that is primarily early onset, associated with progressive limb and gait ataxia, absent tendon reflexes in the legs, axonal sensory neuropathy, dysarthria, muscle weakness, scoliosis, spasticity in the lower limbs, and loss of position and vibration sense.<sup>9,47</sup> Neurodegeneration occurs in the dorsal root ganglia (DRG), with loss of large sensory neurons, as well as degeneration of posterior columns, and atrophy of the corticospinal tracts and spinocerebellar tracts of the spinal cord and the dentate nucleus in the cerebellum. There is also loss of pancreatic islet cells and hypertrophic cardiomyopathy, which is the most common cause of death among FRDA patients.

FRDA is characterized by decreased expression of the frataxin (FXN) protein, from the *FXN* gene on chromosome 9. This is caused by Guanine-Adenine-Adenine (GAA) trinucleotide repeats within intron 1 of the *FXN* gene.<sup>22,41,44,114</sup> In typical FRDA patients the length of the allele with the shorter GAA expansion inversely correlates with FXN levels, age of onset, and rate of disease progression; longer alleles result in earlier onset and a faster progression.<sup>41,44,86</sup> Expanded GAA repeats may form unusual triplex structures, disrupting RNA polymerase and preventing transcription elongation.<sup>8</sup> Epigenetic mechanisms of decreased FXN levels have been observed as regions flanking GAA repeat expansion exhibit marks of condensed heterochromatin. There is also increased methylation of specific CpG sites, reduction of histone H3 and H4

acetylation levels and increased histone H3 lysine 9 (H3K9) trimethylation in FRDA lymphoblasts, peripheral blood, brain and heart tissues.<sup>3,24,55,57</sup>

## 1.2 Frataxin Function

Typical FRDA patients carry less than 10% of control FXN levels, which correlate with disease severity.<sup>41</sup> FXN is a highly conserved mitochondria protein that is important for proper mitochondria function, but the mechanism by which decreased expression leads to disease pathology is unknown. The *FXN* gene is composed of seven exons (exons 1–4, 5a, 5b and 6), with exons 4 and 5a being the most conserved. The crystal structure of FXN, containing amino acid residues 81-210, forms a large, twisted, six-stranded  $\beta$ -antiparallel sheet, flanked by N- and C-terminal  $\alpha$  helices ( $\alpha$ 1 and  $\alpha$ 2). The negatively charged residues on the helical plane are proposed to be involved in iron binding,<sup>1</sup> while the uncharged residues on the surface beta sheet are likely to be responsible for protein–protein interactions.

Frataxin is translated by cytoplasmic ribosomes,<sup>106</sup> and translocated to the mitochondria by an N-terminal mitochondria localization sequence. Upon entry into the mitochondria,<sup>68</sup> FXN undergoes two-step proteolytic cleavage by mitochondria processing peptidase (MPP) to generate the mature protein consisting of amino acids 81-210.<sup>13,25</sup>

Many studies have implicated FXN as a key player in iron metabolism, iron storage and iron-sulfur cluster biogenesis.<sup>23,30,38,60,68,71,80,94,95,110,123</sup> A conserved primary  $\text{Fe}^{2+}$  binding site, with a dissociation constant within the micromolar range (3–55  $\mu\text{M}$ ), involves residues of the acidic ridge localized within the first alpha helix.<sup>32,81,87,123</sup> In addition to Fe binding, FXN interacts with mitochondrial aconitase, ferrochelatase and proteins of the mitochondrial Fe-S cluster machinery.<sup>6,15,50,124</sup> Fe is essential for

metabolic processes including oxygen transport, electron transport, DNA synthesis, redox/non-redox reactions and other cell functions.<sup>42,75</sup> In the central nervous system (CNS) and brain, where energy requirements are high, ATP is in high demand for synaptic transmission and distant axoplasmic transport, all of which involve iron-sulfur enzymes of oxidative metabolism.<sup>31</sup> Fe-S containing proteins play a crucial role in cellular respiration and ATP production, therefore decreased activity has significant effects on mitochondria function.<sup>15,30</sup> FXN's role in iron sulfur cluster biogenesis makes it essential for enzymatic activity of Fe-S containing aconitase and respiratory chain complexes. Consequently, decreased FXN results in decreased aconitase activity, both in cell culture models and *in vivo*,<sup>59,65,91,117,119</sup> and in heart tissues and biopsies of FRDA patients.<sup>65,70,85,97,102</sup>

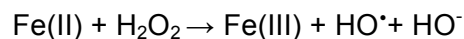
### **1.3 FXN Deficit Leads to Mitochondria Dysfunction**

Overexpression of FXN shows it to be an active participant in pathways of mitochondrial energy conversion and oxidative phosphorylation (OXPHOS), as well as a regulator of the Krebs Cycle.<sup>101</sup> Dysregulation of cell and mitochondrial iron metabolism is a common pathogenic mechanism among neurological diseases; therefore, an emphasis on the role of mitochondria in FRDA pathogenesis has been increasingly explored.<sup>99</sup>

Energy production through oxidative OXPHOS is the primary function of mitochondria for maintaining optimum cellular activity. The electron transport chain, consisting of a series of complexes, transfers electrons from donors to acceptors in order to generate a proton gradient used to produce adenosine triphosphate (ATP) by OXPHOS. It has been suggested that there is a direct interaction between FXN and complex II subunits, suggesting a role for FXN in the electron transport chain.<sup>52,118</sup>

Therefore, FXN deficiency could lead to decreased energy production and mitochondrial respiration. Decreased Complex I, II and III activity has been observed in endomyocardial biopsies of FRDA patients,<sup>102</sup> and FRDA mouse models demonstrate impairment of mitochondrial biogenesis and OXPHOS dysfunction in respiratory chain complexes I, II and IV.<sup>33,76</sup>

OXPHOS is the primary source of reactive oxygen species (ROS),  $O_2^-$  and  $H_2O_2$ . Although produced throughout the cell, 90% comes from mitochondrial respiration.<sup>4,46,58,120</sup> These toxic products of respiration adjust the physiological redox balance leading to oxidative stress.  $O_2^-$  in excess can inactivate Fe-S containing enzymes leading to the release of iron and increased redox-active iron pool. The exact mechanism by which decreased FXN leads to oxidative stress is unknown. It is proposed that iron, which is mobilized by  $O_2^-$  and  $H_2O_2$ , can participate in the Fenton reaction:



to produce a toxic hydroxyl radical ( $HO^{\bullet}$ ). The hypothesis that frataxin deficiency leads to enhanced Fenton reaction as a contributor of FRDA pathogenesis is supported by increased ROS and mitochondrial iron deposits in FRDA tissues.<sup>2,12,16,27,43,61,63,70,88,107,108,111,112,118</sup> Under physiological conditions, superoxide dismutases (SODs) are the first line of defense against ROS, converting  $O_2^-$  into  $H_2O_2$ ,<sup>17</sup> as well as scavenging enzymes and small antioxidant molecules; however, this response was found to be compromised in FRDA patient fibroblasts.<sup>78,93</sup>

Furthermore, energy production and respiratory chain complexes are also important for mitochondria network dynamics. Human fibroblasts carrying genetic changes in the subunits of the respiratory chain complexes show a fragmented

mitochondrial network.<sup>66,67</sup> Few data on the mitochondrial network structure in frataxin-deficient cells are available, and the mitochondrial response to different stresses will depend on the cell type physiology, cell adaptation capacity and biological microenvironment.<sup>53</sup>

## **1.4 Clinical Trials and Therapeutic Strategies**

At present there is no cure or effective treatment for FRDA. Frataxin function remains to be elucidated; current strategies aim to increase FXN expression or target downstream pathways affected secondary to FXN deficiency. High-throughput screening with different cellular models is also being used to search for new drugs.<sup>18</sup>

### *1.4.1 Antioxidants and oxidative phosphorylation*

FXN deficiency causes cells to be highly sensitive to damage caused by oxidative stress, suggesting antioxidants could be a therapeutic approach for FRDA. Idebenone is a short-chain CoQ<sub>10</sub> analogue that acts as an antioxidant by protecting membrane lipids from peroxidation and stimulating OXPHOS and ATP production by carrying electrons from complexes I and II to complex III in the electron transport chain.<sup>84</sup> Idebenone was first identified as a candidate for treatment of FRDA<sup>105</sup> based on its ability to protect the respiratory complex II from iron inactivation and decreased lipoperoxidation. Studies have suggested it improves neurologic functions.<sup>39</sup> Furthermore, treatment of three FRDA patients resulted in reduction of myocardial hypertrophy.<sup>105</sup> Idebenone, even at high doses, appears safe and well-tolerated, however results were not replicated in more systematic trials and it appears to have no effect on disease progression and the neurologic status in patients as compared to placebo.

Treatment of patients with Idebenone or a combination of coenzyme Q<sub>10</sub> (CoQ<sub>10</sub>) with vitamin E to improve mitochondrial function and to reduce oxidative stress has been explored. Vitamin E is a natural antioxidant that is lipid-soluble and highly abundant in nuclear and mitochondrial membranes. CoQ<sub>10</sub> is an electron carrier in the respiratory chain and is involved in the reduction of oxidized vitamin E. When FRDA patients were treated with this combination there was improvement in cardiac and skeletal muscle bioenergetics, however there was no observed benefit on cardiomyopathy.<sup>56</sup>

Other CoQ<sub>10</sub> analogues have been developed such as MitoQ, which specifically targets mitochondria and has been shown to protect patient fibroblasts from endogenous oxidative stress effectively.<sup>62</sup> However, MitoQ does not exchange electrons in the respiratory chain, and cannot be regenerated to stimulate OXPHOS, creating a limitation to this treatment in clinical trials.

#### *1.4.2 Iron chelating strategy*

The pathogenesis of FRDA seems to involve an imbalance in the intracellular accumulation of iron, with mitochondrial accumulation and relative cytosolic depletion. One therapeutic approach for this is iron chelation, which is the current treatment of systemic iron overload diseases. Limitations to iron chelators as a therapeutic include membrane permeability and specific redistribution of iron from mitochondria without compromising overall cellular availability.<sup>98</sup> For example, Desferoxamine chelates iron in the extracellular compartment and cytosol, promoting cellular iron depletion, but has poor membrane penetration and cannot be given orally. Studies also found that it reduces Fe(II) toxicity on mitochondrial complex II, but also decreases aconitase activities and down-regulates frataxin.<sup>10,74,105</sup> Consequently it cannot be used to treat FRDA.



Alternatively, Deferiprone is an iron chelator that localizes to the mitochondria<sup>98</sup>, rapidly distributes in the CNS, crossing membranes, and can penetrate mitochondria to remove excess iron. Deferiprone has a low affinity for iron and less tendency to cause overall iron depletion.<sup>115</sup> It restores mitochondrial redox potential, reduces ROS, prevents apoptosis and increases aconitase activity, without affecting frataxin levels,<sup>51,64</sup> it is well tolerated and can be administered orally. However, worsening of tremor occurred at higher doses and the risk of agranulocytosis remains a threat of deferiprone treatment.

#### *1.4.3 Histone deacetylase inhibitors*

Histone deacetylases (HDACs) inhibitors (HDACi) have been proposed to counteract the chromatin-condensing effect of the GAA repeat expansions and to restore frataxin expression in FRDA. HDACi revert silent heterochromatin to an active chromatin conformation with both positive and negative effects on gene expression.<sup>40,100</sup> Such molecules aim to restore the transcriptional deficit at the *FXN* gene in patients; however, changes in gene transcription could further exacerbate the existing FRDA pathology.

#### **1.5 Frataxin missense mutations**

2-3% of FRDA patients carry a GAA expansion on one FXN allele, and a missense mutation on the other. Many disease-associated missense mutations in the C-terminus end of FXN have been identified, yet few have been characterized *in vivo* or *in situ*. Some are proposed to disrupt mRNA expression (various splice site mutations such as c.165 + 1 G>A and c.384 -2 A>G),<sup>34,109</sup> translation initiation (c.1A>T, c.2T>C, c.2delT, c.3 g>T, c.3G>A), or protein folding (L106S).<sup>7,25,38,48</sup> These should produce little to no functional protein, and their associated phenotype should be severe in conjunction

with a long GAA repeat on the other *FXN* allele. In contrast, R165C, W155R, G130V, and I154F mutations are suspected to produce stable protein. However, R165C and W155R lead to biochemical deficiencies *in vitro*.<sup>14,116</sup> The mechanism behind the disease-causing features of G130V and I154F is less clear, having been suggested to reflect abnormal maturation or dysfunctional FXN in different models.<sup>48</sup>

The phenotype associated with these patients cannot be predicted with such certainty; these patients can have a mild or severe clinical outcome<sup>45</sup> creating a unique platform to understand clinical heterogeneity. Lower processing efficiency or functional alterations caused by the modification of amino acids are proposed contributors to pathogenicity of missense mutations.<sup>25</sup> Impaired protein maturation correlates with impaired protein stability,<sup>25</sup> however, presently there is no consensus regarding the impact of the selected mutant variants upon protein maturation. Therefore, it is important to investigate if these mutant FXN alleles can be properly processed to the mature form in order to assess their presence in mitochondria and ascertain if it correlates with phenotype.

Defining how missense mutations influence FXN's processing and role in energy production and cellular metabolism will help identify pathways that are affected during disease progression and begin to explain the varying phenotypes and establish a genotype-phenotype correlation.

### **1.6 G130V missense mutation**

Of all disease-associated mutations, patients carrying the G130V missense mutation are of most interest because they have less than 5 % of control mature FXN levels but evolve to a milder phenotype than patients with 2 GAA repeats. In a large

cohort of FRDA subjects, those with the G130V mutation have significantly lower occurrence of cardiomyopathy, scoliosis, and diabetes, and they surpass other point mutation carrying subjects on composite performance measures. They demonstrate greater neurological function and decreased disease severity at a similar disease duration.<sup>7,19,34,36,37,45,49,82,83,90,125</sup> Additionally, primary patient fibroblasts from G130V patients grow at rates similar to controls and faster than typical FRDA patients. In chapter 2 I identify the mechanism by which FXN missense mutations result in lower mature FXN<sup>81-210</sup> levels, and in chapter 3 I present a novel FXN missense mutation and the possible mechanism underlying its association with severe FRDA phenotype. Finally in chapter 4, I assess the multiple features of mitochondrial dysfunction associated with severe phenotype in typical FRDA, and compare them to G130V patients in order to understand the molecular mechanisms underlying the milder phenotype.

## **Chapter 2: Selected Missense Mutations Impair FXN Processing**

### **2.1 Abstract**

In typical FRDA, the shortest GAA expanded allele correlates with FXN levels and disease severity, including age of onset and progression rate. The phenotype of patients who carry a GAA expansion on one allele and a missense mutation on the other allele cannot be predicted with certainty; these patients can have a mild or severe clinical outcome,<sup>8</sup> Many missense mutations in the C-terminus of FXN have been identified in FRDA; however, few have been characterized, and the mechanism by which missense mutations lead to disease pathology is not entirely known. With the absence of GAA repeats on the second allele, the mechanism by which FXN missense mutation result in lower mature FXN<sup>81-210</sup> levels must first be understood. I154F, W155R and R165C have been characterized as dysfunctional mutations,<sup>14,116</sup> by *in vitro* assays. G130V, W168R, and G137V are located predominantly on the surface of FXN and their effects on FXN function have not been described.

In this chapter, the effects of FRDA-associated missense mutations on FXN import into the mitochondria by immunocytochemistry and subcellular fractionation, FXN processing from precursor to mature form by western blot, and FXN interaction with MPP by co-immunoprecipitation were investigated. These studies have identified that the effects of disease-associated mutations on FXN processing lead to abnormal FRDA phenotype in mutation selective ways.

## 2.2 Introduction

FXN is important for proper mitochondrial function, but the mechanism by which decreased expression leads to disease pathology is not entirely known.<sup>52</sup> FRDA is most commonly caused by an expansion of a GAA trinucleotide repeat in the first intron of the *FXN* gene on both alleles. 2-3% of FRDA patients carry GAA repeats on one allele accompanied by a point mutation on the other *FXN* allele. In typical FRDA, the length of the shortest GAA expansion correlates with disease severity; longer GAA expansions result in earlier onset and a faster progression.<sup>41,44,86</sup> The phenotype of patients who carry a GAA expansion on one allele and a missense mutation on the other allele cannot be predicted with certainty; these patients can have a mild or severe clinical outcome,<sup>45</sup> creating a unique platform to understand clinical and genetic heterogeneity.

Upon entry into the mitochondria, precursor FXN<sup>1-210</sup> is processed by mitochondria processing peptidase (MPP) into intermediate FXN<sup>42-210</sup>, followed by mature FXN<sup>81-210</sup>. Many missense mutations in the C-terminus of FXN have been identified in FRDA, yet few have been characterized *in vivo* or *in situ*. Some are proposed to disrupt mRNA expression (various splice site mutations such as c.165 + 1 G>A and c.384 -2 A>G),<sup>34,109</sup> translation initiation (c.1A>T, c.2T>C, c.2delT, c.3 g>T, c.3G>A), or protein folding (L106S).<sup>7,25,38,48</sup> These should produce little to no functional protein, and their associated phenotype should be severe in conjunction with a long GAA repeat on the other *FXN* allele. In contrast, R165C, W155R, G130V, and I154F mutations are suspected to produce stable protein. However, R165C and W155R lead to biochemical deficiencies *in vitro*.<sup>14,116</sup> The mechanism behind the

disease-causing features of G130V and I154F is less clear, having been suggested to reflect abnormal maturation or dysfunctional FXN in different models.<sup>48</sup>

Patients that carry missense mutations, despite milder disease severity in many cases, generally have lower FXN protein levels compared to patients with GAA repeat expansions on both alleles<sup>72</sup>, suggesting that the clinical outcome cannot be explained by decreased FXN expression alone. DNA transcription is not affected by point mutations as evidenced by mRNA levels in people carrying a G130V mutation that are comparable to controls.<sup>7</sup> Our hypothesis is that the disease-causing effect of missense point mutations are posttranslational, thus possibly affecting protein processing.

In this chapter I assess the effects of FRDA-associated missense mutations: R165C, W155R, I154F, G130V, G137V, and L106S on FXN import into the mitochondria, processing from precursor to mature form, and interaction with MPP. Selected disease-related FXN missense mutations impair FXN localization, and selected mutations lead to higher levels of partially processed FXN as well as enhanced interactions with mitochondria processing peptidase. I also assess if impaired processing could be overcome by increasing FXN precursor levels. Finally, I examined a large natural history study to investigate whether patients carrying missense point mutations displayed distinct clinical abnormalities that could be related to the altered processing observed *in vitro*. I believe the incompletely processed FXN<sup>42-210</sup> in patients carrying a G130V or I154F mutation carries some residual activity, possibly contributing to the milder phenotype.

## 2.3 Materials and Methods

### 2.3.1 Site-directed mutagenesis

Each FXN mutant was created using the pcDNA3.1 plasmid with wild-type human FXN containing a C-terminus hemagglutinin (HA) tag (Addgene Plasmid #31895) and the Agilent QuikChange XL Site-Directed Mutagenesis Kit.

### 2.3.2 Transfection and immunostaining

Human embryonic kidney (HEK 293) cells were grown on coverslips and transfected via Lipofectamine 2000 reagent with 4  $\mu$ g of DNA (2  $\mu$ g FXN and 2  $\mu$ g mito-GFP). Twenty-four hours after transfection, cells were fixed with 4% paraformaldehyde followed by treatment with blocking buffer containing 5% normal goat serum, 3% Triton X-100, and 1% BSA. Primary antibody to the HA epitope was added at a 1:100 dilution overnight. Alexa Fluor 568 secondary antibody was added at a dilution of 1:100 and cells were imaged by confocal microscopy.

### 2.3.3 Subcellular fractionation and western blot

Following transfection of FXN-mutant constructs, HEK 293 cells were lysed with buffer containing: 150 mmol/L sodium chloride, 1 mmol/L EDTA, 100 mmol/L Tris-HCl, 1% Triton X-100, 1% sodium deoxycholate, 0.1% sodium dodecyl sulfate, and protease inhibitor cocktail (Millipore #539134) 1:1000 at pH 7.4 for 1 h and centrifuged at 150g to collect whole cell lysates. Whole cell lysates were centrifuged at 100g followed by 150g to separate the soluble mitochondria fraction from the cytosolic fraction, and 100g to collect insoluble mitochondria pellet from soluble mitochondria fraction using a

Thermo Scientific Mitochondria Isolation Kit for Mammalian Cells (#89874). The protein concentration of each fraction was determined using a BCA protein assay, and 4  $\mu\text{g}$  of each fraction was loaded on a 12% NuPage gel for electrophoresis, followed by transfer to nitrocellulose membranes. Membranes were blocked with 3% milk for 1 h and incubated with primary HA antibody overnight at 4°C. Membranes were then incubated with secondary HRP-conjugated antibody for 2 h and immunoreactive bands were visualized using luminol-enhanced chemiluminescence (ECL) HRP substrate.

#### *2.3.4 Coimmunoprecipitation and western blot*

Twenty-four hours after transfection, cells were lysed with buffer containing: 150 mmol/L sodium chloride, 1 mmol/L EDTA, 100 mmol/L Tris-HCl, 1% Triton X-100, 1% sodium deoxycholate, 0.1% sodium dodecyl sulfate, and protease inhibitor cocktail (Millipore #539134) 1:1000 at pH 7.4 for 1 h. For coimmunoprecipitation, 2  $\mu\text{g}$  of MPP primary antibody was added to 800  $\mu\text{g}$  of total lysate and rocked for 2 h at 4°C. The lysate and antibody solution was then added to washed Protein G Agarose beads overnight, rocking back and forth at 4°C. The following day the beads, lysate, and antibody solution were centrifuged at 14,000g and washed five times with IP lysis buffer containing: 150 mmol/L sodium chloride, 1 mmol/L EDTA, 100 mmol/L Tris-HCl, 1% Triton X-100, and 0.5% sodium deoxycholate at pH 7.4. Sample buffer (2X) was added to the beads and heated to 100°C for 5 min. The immunoprecipitated proteins were loaded on a 12% NuPage gel. Normal IgG primary antibody was used as a control as well as anti-FXN primary antibody, followed by Trueblot secondary HRP-conjugated antibody (Rockland



#18-8841-31) to detect immunoreactive bands.

### 2.3.5 MG132 Treatment

Transfected cells were treated with 10  $\mu\text{mol/L}$  of MG132, cell-permeable proteasome inhibitor, for 5 h. Following cell lysis, equal amounts of total cell lysate were loaded on a 12% NuPage gel.

### 2.3.6 Fibroblast FXN levels by Western Blot

Primary fibroblasts from healthy controls and FRDA patients with point mutations were lysed in buffer (0.25 mol/L NaCl, 5 mmol/L EDTA, 50 mmol/L HEPES [pH 7.5], 0.1% NP-40, 0.5 mmol/L DTT) supplemented with 0.1% protease inhibitor cocktail (Sigma Aldrich) and kept on ice for 20 min. The lysates were centrifuged at 20,000g for 10 min at 4°C. The clarified supernatants were transferred to fresh tubes and protein concentrations were determined by Bradford assay. A quantity of 75  $\mu\text{g}$  of whole cell lysate were separated by SDS-PAGE and transferred to a PVDF membrane. Immunoblotting was performed with antibodies against FXN (Santa Cruz Biotechnology) and GAPDH (Millipore), and the signals were detected by HRP-mediated chemiluminescence. Densitometry was performed using Image J software (NIH), and the calculated signal ratio of FXN<sup>42-210</sup> to FXN<sup>81-210</sup> in each group is plotted. The bars represent the average signal for each group: CTRL= 5 fibroblast lines ( $n = 13$ ), G130V =3 lines ( $n = 17$ ), and Typical = 7 lines ( $n = 8$ ). The asterisk indicates significant differences as determined by Student's t-test ( $P < 0.05$ ).

### 2.3.7 Quantification and statistical analysis

Image J Software was used to quantify FXN levels on western blots and is represented as mean  $\pm$  SEM. Two-tailed Student's t-test was used to compare mutants to WT. Significance was set at  $P < 0.05$ . Image J software was also used to calculate Pearson's correlation coefficient for quantification of colocalization in immunofluorescence images.

### 2.3.8 Clinical measures

Clinical measure results were derived from a long-standing natural history study from 12 American and Australian sites.<sup>92</sup> In this study, data is collected annually on clinical features of > 900 individuals with FRDA. Data from the baseline cross sectional visits were used in this study including overall medical history and scores on the Friedreich Ataxia Rating Scale (FARS) (a quantified neurological exam); Ataxia Staging scale (a disability score); the Timed 25-Foot Walk (T25FW), scored as the reciprocal (a simple performance test of walking); 9-Hole Peg Test (9HPT), scored as the reciprocal (a simple test of hand function); Contrast Letter Acuity test, the sum of the number of letters read on each of three Sloan charts (a quantitative test of vision); and an Activities of Daily Living (ADL) scale. All these measures capture progressive neurological dysfunction in FRDA. The performance measures were also transformed into Z-scores to create composite scores as reported previously. The  $Z_2$  composite is the sum of the Z-scores from T25FW and 9HPT. The  $Z_3$  composite is the sum of Z-scores from T25FW, 9HPT, and overall vision tests.

## 2.4 Results

### 2.4.1 Selected FRDA-associated missense mutations decrease FXN<sup>81-210</sup> levels, but do not impair FXN association with mitochondria

To determine the effects of FRDA-associated missense mutations on FXN import into the mitochondria, FXN variants containing a C-terminal HA tag were cotransfected with mito-GFP in HEK 293 cells. Levels of the FXN<sup>81-210</sup> form of I154F and G130V are lower as determined by western blot compared to WT, while no detectable exogenous FXN<sup>81-210</sup> was detected following transfection of G137V and L106S constructs (Fig. 2.1). Confocal microscopy imaging was used to determine localization of the exogenous FXN proteins. R165C and W155R co-localize with mito-GFP and have FXN immunoreactivity comparable to WT (Fig. 2.2A). I154F, G130V, and G137V colocalize with mito-GFP but have lower FXN immunoreactivity compared to FXN<sup>WT</sup> (Fig. 2.2B). Finally, transfection of L106S leads to no FXN immunoreactivity (Fig. 2.2C). All expressed mutant proteins colocalize with mito-GFP with a Pearson's correlation coefficient greater than 0.98. While R165C and W155R have increased immunoreactivity compared to I154F, G130V, and G137V, the I154F, G130V, and G137V proteins retain their mitochondrial localization.

### 2.4.2 Selected FRDA-associated missense mutations impair processing from FXN<sup>42-210</sup> to FXN<sup>81-210</sup>

To investigate further the decrease in FXN<sup>81-210</sup> levels of particular FXN-mutant proteins, subcellular fractionation and separation of the soluble mitochondrial fraction and the insoluble mitochondrial pellet was performed. Consistent with immunocytochemistry results, transfection of R165C or W155R leads to FXN<sup>81-210</sup> levels

comparable to levels of FXN<sup>WT</sup>, while transfection of I54F or G130V produces lower levels of FXN<sup>81-210</sup> (Fig. 2.3A and 2.3B). While I154F or G130V lead to low FXN<sup>81-210</sup> levels, expression of these mutant proteins leads to an increased level of FXN<sup>42-210</sup> (Fig. 2.3A and C), suggesting these FXN variants are not processed readily from FXN<sup>42-210</sup> to the FXN<sup>81-210</sup> form. Furthermore, these variants also have increased ratios of insoluble to soluble FXN<sup>42-210</sup> (Fig. 2.3E-G), suggesting these proteins remain associated with the insoluble inner mitochondrial membrane rather than being released into the soluble portion of the mitochondrion.

#### *2.4.3 Missense mutations FXN<sup>I154F</sup> and FXN<sup>G130V</sup> enhance the association of FXN<sup>42-210</sup> with MPP*

To examine the mechanism by which I154F and G130V impair FXN processing, FXN-mutant proteins were co-immunoprecipitated to study the strength of the interaction between FXN and MPP. The FXN<sup>42-210</sup> forms of I154F and G130V are more readily co-immunoprecipitated by anti-MPP than the FXN<sup>42-210</sup> form of WT, R165C, and W155R proteins (Fig. 2.4), suggesting stronger attachment between these variants and MPP.

#### *2.4.4 Increasing FXN<sup>G130V</sup> and FXN<sup>I154F</sup> FXN<sup>1-210</sup> levels does not increase FXN<sup>81-210</sup> levels*

Traditional therapies for FRDA include several strategies designed to increase FXN levels. To model this approach, transfected cells were treated with 10  $\mu$ mol/L MG132, a proteasome inhibitor, to increase FXN<sup>1-210</sup> levels in an effort to overcome impaired FXN processing. While G130V and I154F FXN<sup>1-210</sup> levels increased, as did FXN<sup>42-210</sup> levels, MG132 treatment did not increase FXN<sup>81-210</sup> levels (Fig. 2.5).

This suggests that amelioration of these missense mutations cannot be achieved with simple overexpression of precursor FXN, and that there is a true impediment to processing of these mutants to the FXN<sup>81-210</sup> form.

#### *2.4.5 Impaired FXN processing from FXN<sup>42-210</sup> to FXN<sup>81-210</sup> occurs in fibroblasts from FRDA patients with FXN<sup>G130V</sup>*

To analyze the significance of these findings in patient-derived cells and examine the processing of native FXN, western blots were performed on whole cell extracts prepared from control (CTRL) and FRDA G130V primary patient fibroblasts. Endogenous FXN<sup>42-210</sup> and FXN<sup>81-210</sup> FXN levels were detected and expressed as a ratio of FXN<sup>42-210</sup>/FXN<sup>81-210</sup> (Fig. 2.6A). The ratio of FXN<sup>42-210</sup> to FXN<sup>81-210</sup> is increased in FRDA G130V patient fibroblasts compared to controls ( $P < 0.05$ ). Patient fibroblasts were also immunostained with antibodies to FXN and mitofusin. FRDA G130V patient fibroblasts contain large globular structures (Fig. 2.6B) consistent with the increased insoluble FXN<sup>42-210</sup> form detected by western blot and overexpression studies.

#### *2.4.6 FRDA patients with FXN<sup>G130V</sup> have milder disease features and slower disease progression compared to other heterozygous FRDA patients*

We then sought to establish whether patients carrying missense point mutations displayed distinct clinical abnormalities that could be related to the altered processing observed in vitro. Heterozygous (HTZ subjects) FRDA patients, with a missense mutation on one FXN allele and GAA expansion on the other, and typical homozygous (HMZ subjects) FRDA patients, with GAA expansions on both FXN alleles, have different clinical profiles when examined in a large natural history study (Table 2.1). In addition, patients carrying G130V mutations have significantly lower occurrence of

cardiomyopathy, scoliosis, and diabetes, the most severe components of the disease, compared to other HTZ subjects (Table 2.2). Furthermore, clinical measures at baseline exam including ataxia stage, activities of daily living (ADL) scores, 9HPT-1, T25FW-1, Vision, 9HPT, Z2, and Z3 were significantly worse in other HTZ subjects, even though the groups were of similar disease duration, suggesting a less severe phenotype in G130V patients (Table 2.2). Patients with an I154F mutation fell between the phenotypic severity of G130V and other point mutations analyzed.

## 2.5 Discussion

In this chapter, FRDA-causing mutations G130V and I154F decrease FXN<sup>81-210</sup> levels, but do not impair FXN localization to mitochondria. G130V and I154F appear to impair FXN processing from FXN<sup>42-210</sup> to FXN<sup>81-210</sup>, as well as enhance binding of FXN<sup>42-210</sup> to MPP. This impaired processing is also observed in primary fibroblasts from FRDA patients with a G130V mutation. Increasing G130V and I154F precursor levels does not lead to an increase in FXN<sup>81-210</sup> levels, but does increase levels of FXN<sup>42-210</sup>. These are all consistent with a defect in peptide processing of these forms being a pathogenic mechanism in patients carrying these mutations. In addition, these two forms, especially G130V, are associated with milder features of FRDA than other point mutations or expanded GAA repeats, suggesting that these mild phenotypes may reflect the underlying FXN biochemistry.

In heterologous systems, disease-associated mutations in FXN are abnormal in several mutation selective ways. The inability to detect L106S and G137V by immunostaining and western blot supports modeling studies suggesting that mutations residing within the protein core decrease protein stability.<sup>48</sup> *In vitro* functional studies have also characterized R165C and W155R as dysfunctional mutations, causing decreased binding of FXN to Fe-S cluster assembly complex.<sup>14,116</sup> Moreover, R165C and W155R had levels of FXN<sup>81-210</sup> that were comparable to WT, and there was no evidence for impaired processing of these two mutant forms from FXN<sup>42-210</sup> to FXN<sup>81-210</sup>. Further functional studies *in vivo* may provide a correlation between the extent of dysfunction in these two FXN-mutant proteins and severity of disease outcome.

Abnormalities in FXN processing have been explored mostly in yeast and bacteria expression systems.<sup>25,26,54,69</sup> Here, we show an increased level of the FXN<sup>42-210</sup> form in disease-associated missense mutations associated with milder phenotypes, not only in overexpression studies using mammalian systems, but also in primary fibroblasts from FRDA patients. FRDA patients who carry G130V express lower FXN<sup>81-210</sup> levels than typical FRDA patients in fibroblasts, cheek swabs, and blood,<sup>72</sup> yet have a milder clinical phenotype (Tables 2.1 and 2.2). In a large cohort of FRDA subjects, even though those with the G130V mutation have similar disease duration, they have significantly better FARS and ADL scores than individuals with other point mutations. FRDA G130V patients also have significantly lower occurrence of cardiomyopathy, scoliosis, and diabetes, and they surpass other point mutation carrying subjects on composite performance measures. As suggested in single cases previously, this demonstrates that FRDA patients with G130V demonstrate greater neurological function and decreased disease severity at a similar length of disease duration.

<sup>7,19,34,36,37,45,49,82,83,90,125</sup> Patients with I154F mutations have clinical severities intermediate between other patients with point mutations and G130V patients, matching the data from cellular models of the molecular consequences of these mutants.

One explanation for the milder phenotype in patients carrying a G130V or I154F mutation is that the incompletely processed FXN<sup>42-210</sup> carries some residual activity. In these mutants, this form is located in the mitochondria, and others suggest that FXN<sup>42-210</sup> can perform Fe-S cluster synthesis as well as participate in cysteine desulfurase activity as efficiently as FXN<sup>81-210</sup>.<sup>73,117</sup> Thus, the higher levels of FXN<sup>42-210</sup> associated with G130V could lead to the mild phenotype of patients with G130V if this intermediate form is functional. Alternatively, it is possible that a small but clinically significant amount



of the FXN<sup>42-210</sup> form is slowly converted to the mature form, leading to the milder phenotype in patients carrying G130V mutations compared with other mutations that yield absolutely no mature FXN. Further experiments examining the functional abilities of the FXN<sup>42-210</sup> form of endogenous G130V may help clarify these possibilities. Overall, the present study, in agreement with modeling studies and those in lower animal expression systems, identifies multiple mechanisms in mammalian heterologous systems by which FXN point mutations can lead to FRDA.

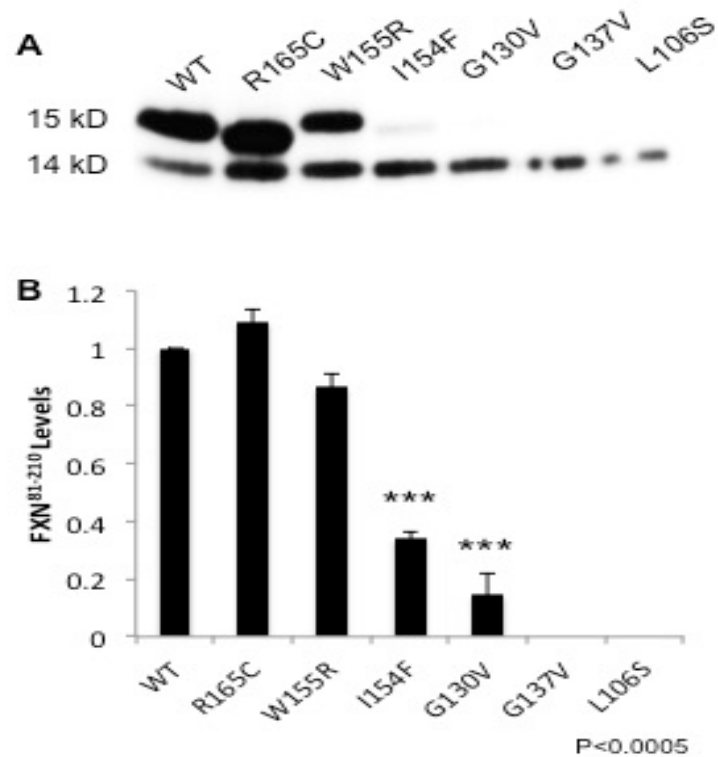


Figure 2.1 FXN levels of disease-associated missense mutations. **A.** Western blot of whole cell lysates collected from HEK 293 cells transfected with FXNWT, FXNR165C, FXNW155R, FXNI154F, FXNG130V, FXNG137V, and FXNL106S. An anti-FXN antibody was used to detect both exogenous FXN81–210 (15 kD) and endogenous FXN81–210 (14 kD) levels after transfection. **B.** Quantification of exogenous FXN levels was normalized to FXNWT and endogenous FXN. Endogenous FXN serves as a loading control. (\*\*\*) = P < 0.0005.

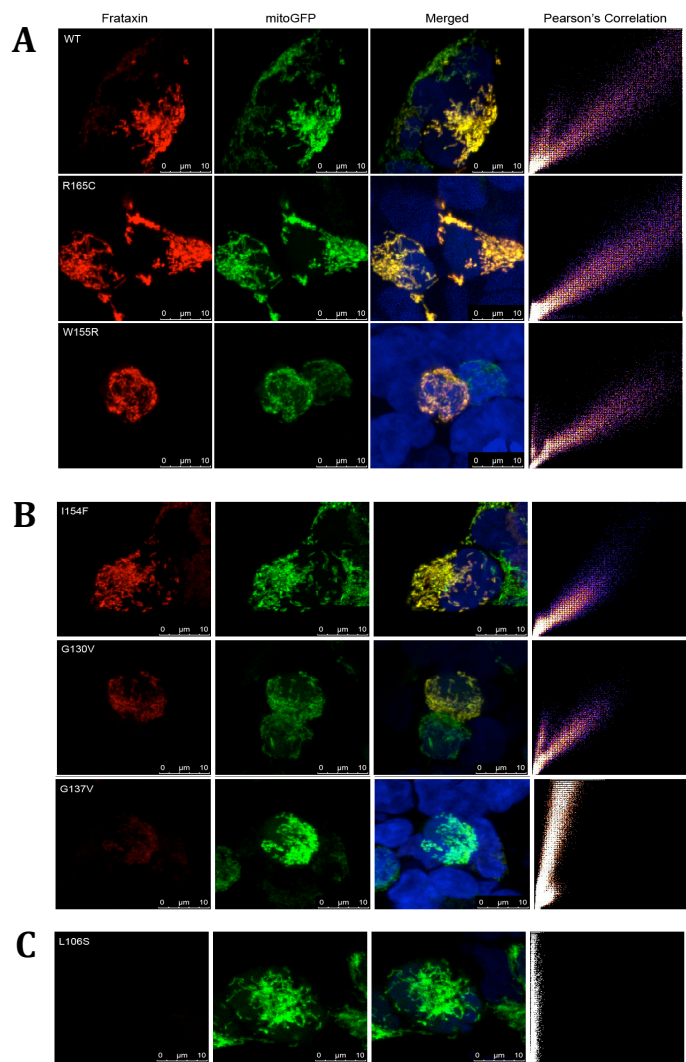


Figure 2.2 Selected FRDA-associated missense mutations do not impair FXN association with mitochondria. Confocal microscopy images of HEK 293 cells cotransfected with mutant FXN constructs and mito-GFP, fixed, and stained using a primary anti-HA antibody to detect exogenous FXN only and secondary antibody Alexa Fluor 568 (FXN). DAPI was also used as a nuclear stain. **A.** FXNWT, FXNR165C, and FXNW155R. **B.** FXN154F, FXNG130V, and FXNG137V. **C.** FXNL106S. Pearson's correlation scatter plots of red and green signal intensities for each mutant were generated using Image J Software.

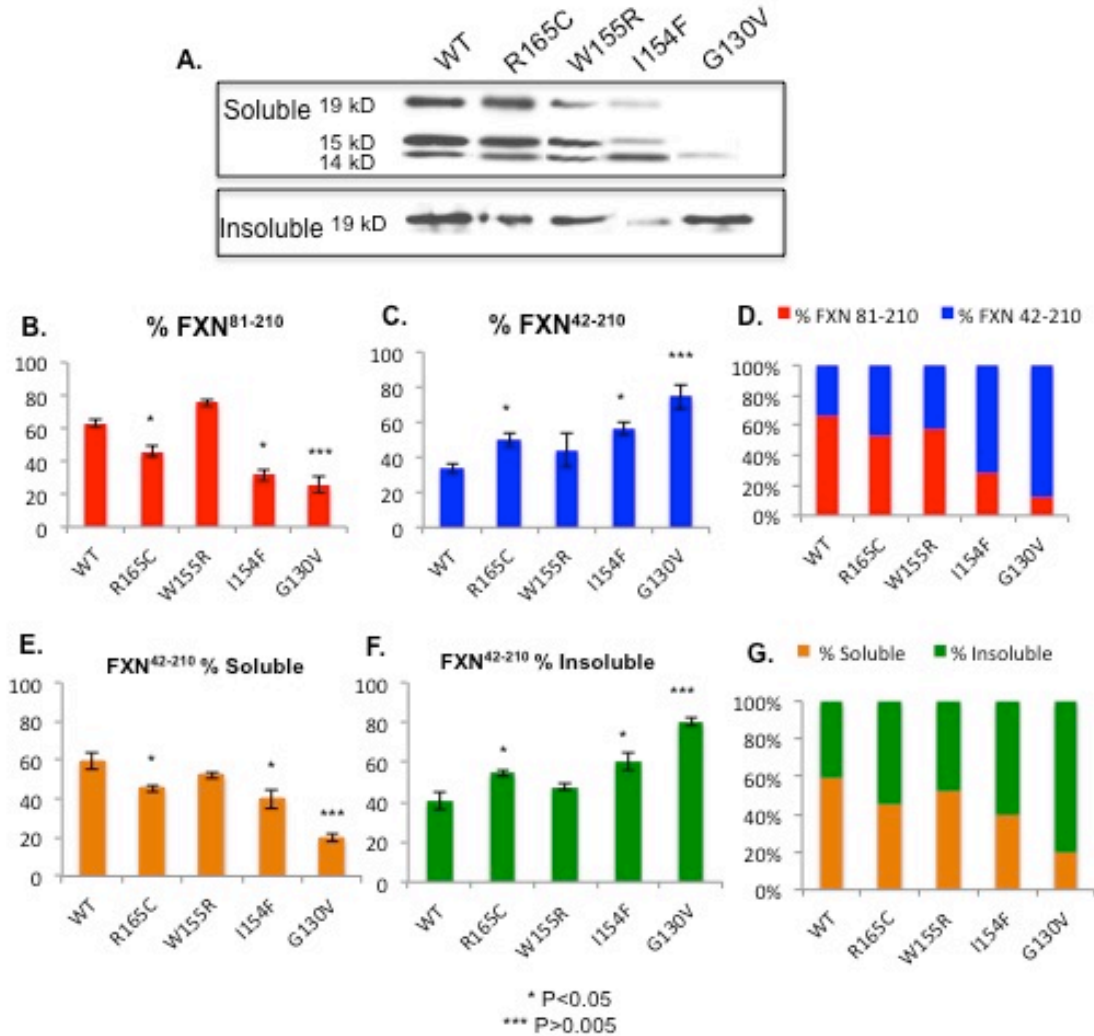


Figure 2.3 Selected FRDA-associated missense mutations impair processing from FXN42–210 to FXN81–210. Following transfection of mutant constructs in HEK 293 cells, whole cell lysates were centrifuged to perform subcellular fractionation of soluble mitochondria fraction and insoluble mitochondrial pellet. **A.** FXN levels were detected by western blot using an anti-FXN antibody. Anti-SDHA antibody was used to detect SDHA as a mitochondria marker and loading control. The soluble mitochondria fraction includes: exogenous FXN42–210 (19 kD), exogenous FXN81–210 (15 kD), endogenous FXN81–210 (14 kD), and SDHA (70 kD). The insoluble mitochondria pellet includes: exogenous FXN42–210 (19 kD) and SDHA (70 kD). **B.** Percent FXN81–210 of total FXN. **C.** Percent FXN42–210 of total FXN. **D.** Total FXN. **E.** Percent soluble FXN42–210. **F.** Percent insoluble FXN42–210. **G.** Total FXN42–210. (\*) = P < 0.05 and (\*\*\*) = P < 0.005

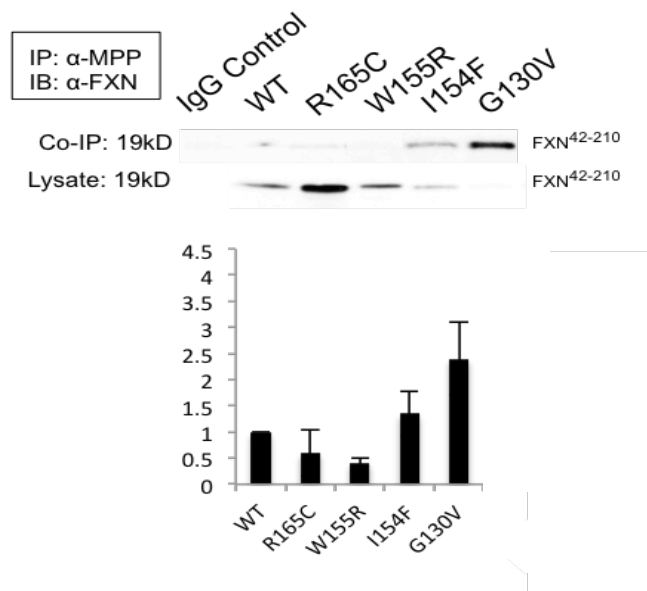


Figure 2.4. Missense mutations FXNI154F and FXNG130V enhance the association of FXN42–210 with MPP. Whole cell lysates from transfected HEK 293 cells were immunoprecipitated with anti-MPP antibody and immunoblotted with primary anti-FXN antibody. The same whole cell lysates were used as inputs for quantification analysis. Western blot was used to detect FXN pulled down by anti- MPP. The Co-IP 19 kD blot represents immunoprecipitated FXN42-210. The lysate 19 kD blot represents total FXN42-210 in whole cell lysate. The graph represents fold change of FXN mutant interaction with MPP compared to FXNWT.

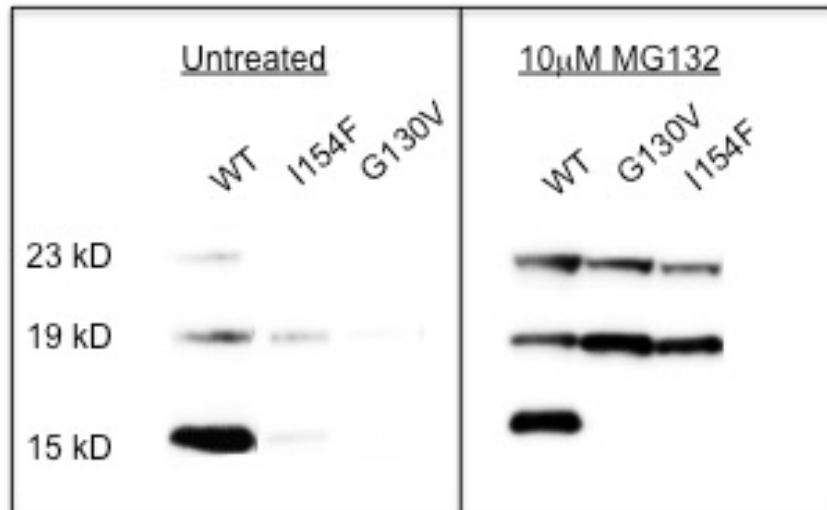


Figure 2.5 Increasing FXNG130V and FXNI154F FXN1–210 levels does not increase FXN81–210 levels. Following transfection of HEK 293 cells with mutant FXN constructs, cells were treated with 10 μmol/L MG132 proteasome inhibitor for 5 h followed by cell lysis. Exogenous FXN1–210 (23 kD), FXN42–210 (19 kD), and FXN81–210 (15 kD) levels, before and after treatment, were detected by western blot using a primary anti-HA antibody.

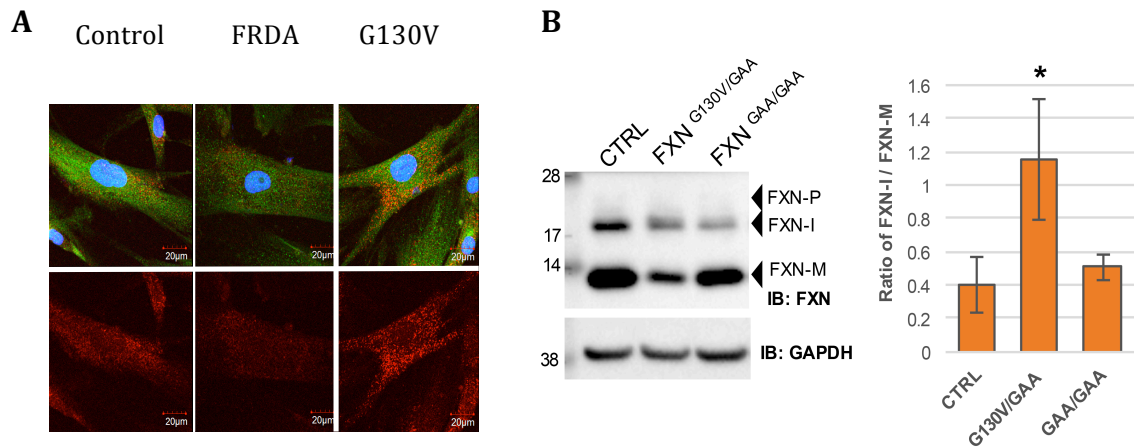


Figure 2.6. Impaired FXN processing from FXN42–210 to FXN81–210 occurs in fibroblasts from FRDA patients with FXNG130V. FXN levels were quantified by western blot using whole cell extracts from control (CTRL), FRDA, and G130V patient fibroblasts. CTRL= 5 fibroblast lines (n = 13), G130V =3 lines (n = 17), and Typical = 7 lines (n = 8). **A.** FXN42–210 (18 kD), and FXN81–210 (13 kD) levels from control (CTRL), G130V, and typical FRDA were detected from whole cell extracts by western blot using an anti-FXN antibody. Detection of GAPDH serves as a loading control. FXN levels are quantified and expressed as a ratio of FXN42–210 to FXN81–210. (\*) = P < 0.05. **B.** Confocal microscopy images of patient fibroblasts (CTRL, FRDA, and G130V) that were fixed and stained using primary anti-FXN (red) and primary anti-mitofusin antibodies (green). Secondary antibodies included Alexa Fluor 568 (FXN) and Alexa Fluor 488 (mitofusin). DAPI was also used as a nuclear stain.

	HMZ	HTZ
N	741 (96%)	32 (4%)
Age of Onset	13.8	10.7*
BL age	26.5	24
Recent age	30	27.3
Duration	16.2	16.6
Sex (%female)	49.40%	43.80%
Non-ambulatory	50.20%	46.90%
Cardiomyopathy	57.80%	34.6%*
Scoliosis	82.40%	73.10%
Diabetes	5.50%	26.9%*
FARS	69.4	61.7
Stage	4	3.9
ADL	16.3	13.4
9HPT-1 (high = less severe)	0.014	0.025*
T25FW-1 (high = less severe)	0.055	0.062
Vision	105.3	100.6
Z2 (high = less severe)	-0.09	0.48*
Z3 (high = less severe)	-0.08	0.26

\*p<0.05

Table 2.1 Clinical measures comparing FRDA homozygous and heterozygous patients. Patients who were heterozygous (HTZ) for the GAA repeat (those carrying point mutations or deletions) had similar disease durations to those who were homozygous (HMZ), but, aside from age of onset and presence of diabetes, were less severely affected than homozygous patients. This was particularly true for measures containing upper extremity function such as the nine-hole peg test and the Z2 score.\*P < 0.05



	G130V	I154F	Other HTZ
N	9	3	18
Age of Onset (years)	10.8	11	11.5
BL age (years)	21.4	22.6	11.5
Recent age (years)	23.4	25	23.5
Duration (years)	12.4	14	15.9
Sex (%female)	44	67	44
Cardiomyopathy (%)	12.5	0	50
Scoliosis (%)	50	100	78.6
Diabetes (%)	12.5	6.7	35.7
FARS	40.6	54.3	72.4
Stage	2.4	3.5	4.5
ADL	5.8	8	17.5
9HPT-1 (high = less severe)	0.044	0.029	0.015
T25FW-1 (high = less severe)	0.139	0.117	0.026
Vision	127.8	125.5	85.3
Z2 (high= less severe)	2.03	0.99	-0.21
Z3 (high = less severe)	1.55	0.79	-0.38

Table 2.2 FRDA patients with FXNG130V have milder disease features and slower disease progression compared to other heterozygous FRDA patients. Clinical data were collected from a large natural history study of FRDA, including data on medical history, genetic status, disability and activity of daily living (ADL) status, a quantitative neurological exam (designated the Friedreich ataxia rating scale [FARS]), performance measures, and two performance measure composites. When we fractionated the heterozygous patients into patients those carrying G130V versus I154F versus others, the G130V patients were markedly less affected. I154F patients had levels of dysfunction between G130V and other heterozygous patients.

## **Chapter 3: Identification of a Novel Missense Mutation- FXN<sup>W168R</sup>**

### **3.1 Abstract**

Friedreich's Ataxia, a slowly progressive ataxia characterized by decreased expression of the frataxin (FXN) protein, is caused by GAA trinucleotide repeats within intron 1 of the *FXN* gene in 98% of patients. Two percent of patients with FRDA carry one expanded GAA repeat in conjunction with a point mutation. In general, patients with point mutations carry even lower FXN levels than typical FRDA patients. The mechanism by which disease-associated missense mutations lead to disease pathology is unclear, but occurs in mutation-selective ways by affecting protein folding, processing, or function.

In this chapter the novel disease-causing W168R missense mutation is introduced and its effects on FXN import into the mitochondria by immunocytochemistry and subcellular fractionation, FXN processing from precursor to mature form by western blot, and FXN interaction with MPP co-immunoprecipitation were investigated. These studies have identified that W168R impairs FXN processing as a contributor to severely low FXN levels, and a severe phenotype.

### 3.2 Introduction

Typical FRDA is characterized by decreased expression of the frataxin (FXN) protein, from the *FXN* gene on chromosome 9, caused by the presence of expanded GAA trinucleotide repeats within intron 1 on both alleles. FXN is crucial for proper mitochondrial function and iron-sulfur cluster biogenesis, but the mechanism by which decreased protein expression leads to disease pathology is not fully known. 2% of patients carry expanded GAA repeats on one allele, and a point mutation on the other allele. These patients generally have lower FXN levels compared to typical FRDA patients<sup>29,72</sup>. As intronic and frame shift point mutations lead to absence of functional frataxin<sup>7,25,34,38,48,109</sup>, the phenotype in such patients is usually severe. In contrast patients with missense mutations can have a mild or severe clinical outcome depending on the exact mutation and the length of the GAA repeat on the opposite allele<sup>34,45,48,83,109</sup>. *In vitro* studies allow one to distinguish between those affecting frataxin processing and those altering overall levels (due to folding, RNA splicing or other severely pathogenic processes). *In vitro* studies show that the specific location of missense mutations within the protein structure has effects on protein folding (L106S)<sup>7,25,38,48</sup> and decreased participation in Fe-S cluster biogenesis (R165C, W155R)<sup>14,116</sup>.

A patient who carries a novel W168R missense mutation and 1133 expanded GAA repeats on the opposite allele is presented in this chapter. The patient has extremely low levels of mature FXN<sup>81-210</sup> and an especially severe phenotype. The non-conservative W168R mutation is an amino acid switch from an aromatic, non-polar tryptophan to a basic, electrically charged arginine at amino acid position 168 on Beta-sheet 5 of the human FXN crystal structure. Based on the amino acid position 168, it is

anticipated that W168R destabilizes FXN and alters levels by misfolding. Our hypothesis is that the W168R mutation impairs FXN processing, thus leading to very low FXN levels. The effects of W168R on FXN import into the mitochondria, subcellular localization, and interactions with mitochondria processing peptidase (MPP) were first assessed. W168R is expressed predominantly as the intermediate FXN<sup>42-210</sup> form, with little to no expression of the mature FXN<sup>81-210</sup> form consistent with patient samples, and its localization to the mitochondria is not impaired. Increasing mature FXN levels with W168R by modeling traditional therapies was also assessed, and indeed it did not. We believe patients with W168R will require alternative approaches to repair FXN processing from intermediate to mature form in order to increase FXN levels. Furthermore, in addition to impairing FXN processing, we expect the W168R mutation has another feature that alters FXN function, leading to a more severe phenotype.

### **3.3 Materials and Methods**

#### *3.3.1 Transfection and Immunostaining*

W168R was created using Addgene XL Site-Directed Mutagenesis Kit and primers to pcDNA3.1-hFratxin-HA (Plasmid #31895). Human Embryonic Kidney (HEK) cells were co-transfected with 4ug of FXN and mitoGFP cDNA via Lipofectamine 2000 reagent. 24 hours after transfection, cells were fixed with 4% Paraformaldehyde followed by treatment with blocking buffer containing 5% normal goat serum, 3% Triton X-100, and 1% BSA. Primary antibody to the HA epitope was added at a 1:1000 dilution overnight. Alexa Fluora 568 secondary antibody was added at a dilution of 1:1000 and cells were imaged by confocal microscopy.

#### *3.3.2 Transfection, Subcellular Fractionation, and Western Blot*

Following transfection of FXN mutants, HEK cells were centrifuged at 150 x g to collect whole cell lysates. The soluble mitochondria fraction and insoluble mitochondria pellet were collected using Thermo Scientific Mitochondria Isolation Kit for Mammalian Cells (#89874). Protein concentration of each fraction was determined using BCA Protein Assay and each fraction was loaded on a 12% NuPage Gel for electrophoresis, followed by transfer to nitrocellulose membranes. Membranes were blocked with 3% Milk for 1 hour and incubated with primary HA-antibody overnight at 4 °C. Membranes were then incubated with secondary HRP-conjugated antibody for 1 hour and immunoreactive bands were visualized using luminol-enhanced chemiluminescence (ECL) HRP substrate.

### *3.3.3 MG132 Treatment*

HEK cells were transfected with FXN<sup>WT</sup> and W168R mutants via Lipofectamine 2000 reagent. 24 hours after transfection cells were treated with 10mM MG132 for 5 hours followed by cell lysis. Equal amounts of total lysate were loaded on a 12% NuPage gel.

### *3.3.4 Quantification and Statistical Analysis*

Image J Software was used to quantify FXN levels on western blots and is represented as mean  $\pm$  S.E.M. Two-tailed student's t-test was used to compare W168R to WT. Significance was set at  $P < 0.05$ . Image J software was also used to calculate Pearson's correlation coefficient for quantification of co-localization in immunofluorescence images.

## 3.4 Results

### 3.4.1 Case History

A six-year old boy evaluated for ataxia, was historically smaller in size and slower to progress developmentally than his fraternal twin brother. His height and weight were consistently below the 1% percentile since birth. Hypotonia, decreased stamina, clumsiness, and balance difficulties were noted around age two. When symptoms failed to improve by age three, orthotics was prescribed, and physical therapy was initiated. At age four, he was diagnosed with mild concentric left ventricular hypertrophy, diastolic dysfunction as well as a scoliosis of 14 degrees. Initial testing included standard blood work, a brain MRI, and ophthalmologic evaluation. Genetic testing performed to rule out mitochondrial diseases ultimately rendered a diagnosis of Friedreich ataxia with GAA repeats of 19 and 1133 and a novel W168R missense mutation. The subject's father carried this mutation and his mother carried an expanded GAA repeat.

### 3.4.2 *W168R impairs FXN processing from intermediate to mature form, but does not impair FXN association with mitochondria.*

Based on western blotting of equal protein lysates, W168R is expressed predominantly as the FXN<sup>42-210</sup> form with nearly no detectable FXN<sup>81-210</sup> immunoreactivity compared to WT (Figure 3.1). To determine the effects of the W168R missense mutation on FXN import into the mitochondria, the W168R variant containing a C-terminal HA tag was co-transfected with mitoGFP in Human Embryonic Kidney (HEK 293) cells. Confocal microscopy images with an antibody to the HA epitope, to detect exogenous FXN only, show W168R co-localization with mitoGFP, but with lower levels of FXN

immunoreactivity compared to WT (Figure 3.2). This data suggests that although W168R decreases mature FXN levels, the immunoreactivity that remains is still associated with mitochondria. To further examine the effects of W168R on FXN processing, co-immunoprecipitation of W168R and MPP shows enhanced interactions with the FXN<sup>42-210</sup> form compared to WT (Figure 3.3). This is further demonstrated through subcellular fractionation in which the FXN<sup>42-210</sup> form of W168R is present in both soluble and insoluble mitochondria fractions (Figure 3.4). This suggests that W168R impairs FXN processing from the FXN<sup>42-210</sup> to FXN<sup>81-210</sup> form, and is retained with MPP at the inner mitochondria membrane.

### *3.4.3 Increasing FXN<sup>W168R</sup> precursor levels does not lead to an increase in mature FXN levels.*

Traditional therapies for FRDA involve increasing FXN levels. To model this, transfected cells were treated with 10mM MG132 protease inhibitor to increase precursor FXN levels in an effort to overcome the impaired FXN processing by W168R. W168R precursor levels increased, as did FXN<sup>42-210</sup> levels, but not FXN<sup>81-210</sup> levels (Figure 3.5). This suggests that increasing mature FXN levels for W168R will require alternative approaches to repair FXN processing from intermediate to mature form.



### 3.5 Discussion

In this chapter a novel W168R FXN mutation is presented in a patients with a single long GAA repeat on the other allele, and very low mature FXN<sup>81-210</sup> levels with early onset and significant disease progression. W168R is expressed predominantly as the intermediate FXN<sup>42-210</sup> form, with little to no expression of the mature FXN<sup>81-210</sup> form, but its localization to the mitochondria is not impaired. The G130V mutation, associated with milder phenotype, is also expressed predominantly as the intermediate FXN<sup>42-210</sup> form, with very low mature FXN<sup>81-210</sup> form. However, the G130V mutation may provide intermediate FXN functional capacity to compensate for lower mature levels. Alternatively, low levels of G130V mature FXN levels may be sufficient to ameliorate the phenotype, while W168R, one alpha helix turn away from the dysfunctional R165C mutation, is in a unique position to impair both processing and potentially FXN functionality, leading to a severely deficient form of abnormal frataxin and severe phenotype. This suggests that the extremely low levels of mature frataxin produced from W168R are no different than that from G130V, and that phenotypic differences related to such mutations are most likely to reflect other abnormalities in the different mutants.

Additionally, we investigated if traditional therapies for increasing FXN levels would be relevant to patients with W168R. Increasing precursor levels does not lead to an increase in mature FXN<sup>81-210</sup> levels. One explanation is that W168R slows down the FXN processing rate in such that increased precursor FXN levels never get processed to the mature form, possibly by blocking or inhibiting the second MPP cleavage site. In summary, this data suggests that patients with W168R will require alternative approaches to repair FXN processing from intermediate to mature form in order to

increase FXN levels and treat the disorder in a disease-modifying manner. Furthermore, functional studies will be required to ascertain the mechanism by which W168R affects FXN function and leads to severe phenotype.

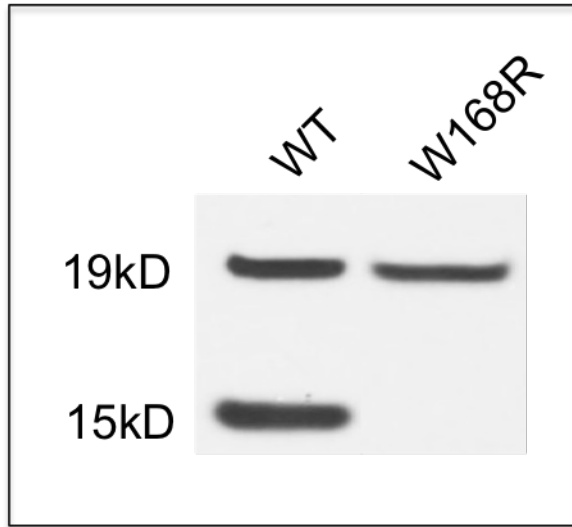


Figure 3.1 W168R decrease FXN<sup>81-210</sup> levels. Western blot of whole cell lysates collected from HEK 293 cells transfected with FXNWT and FXNW168R. An anti-HA antibody was used to detect exogenous FXN81-210 (15 kD) FXN81-210 levels after transfection.

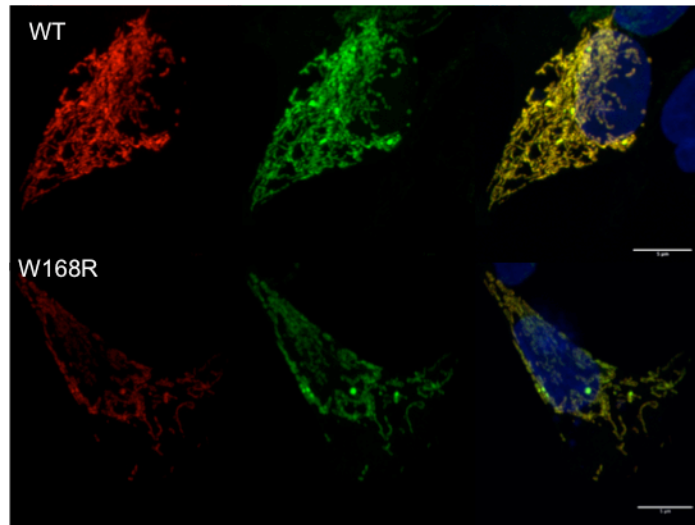


Figure 3.2 W168R does not impair FXN association with mitochondria. Confocal microscopy images of HEK 293 cells cotransfected with mutant FXN constructs and mito-GFP, fixed, and stained using a primary anti-HA antibody to detect exogenous FXN only and secondary antibody Alexa Fluor 568 (FXN). DAPI was also used as a nuclear stain.

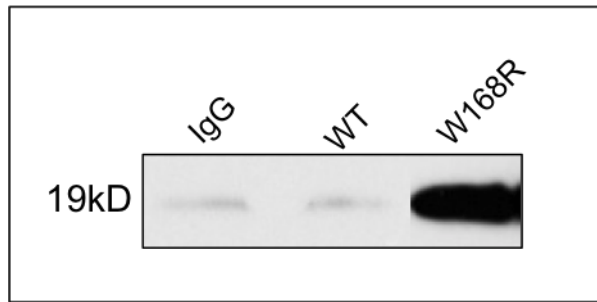


Figure 3.3 W168R enhances the association of FXN<sup>42-210</sup> with MPP. Whole cell lysates from transfected HEK 293 cells were immunoprecipitated with anti-MPP antibody and immunoblotted with primary anti-HA antibody. Western blot was used to detect FXN pulled down by anti- MPP. The Co-IP 19 kD blot represents immunoprecipitated FXN42-210.

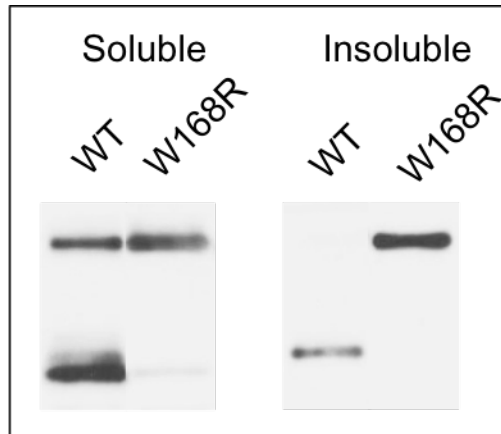


Figure 3.4 W168R impairs processing from FXN<sup>42-210</sup> to FXN<sup>81-210</sup>. Following transfection of mutant constructs in HEK 293 cells, whole cell lysates were centrifuged to perform subcellular fractionation of soluble mitochondria fraction and insoluble mitochondrial pellet. FXN levels were detected by western blot using an anti-HA antibody.

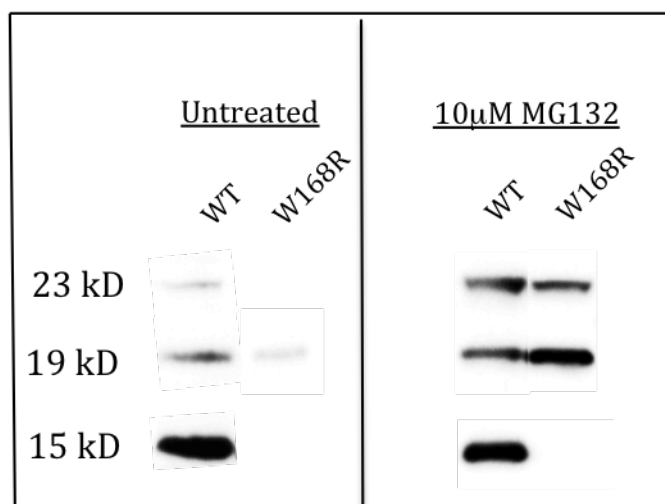


Figure 3.5 Increasing W168R FXN<sup>1-210</sup> levels does not increase FXN<sup>81-210</sup> levels. Following transfection of HEK 293 cells with mutant FXN constructs, cells were treated with 10  $\mu$ M MG132 proteasome inhibitor for 5 h followed by cell lysis. Exogenous FXN1-210 (23 kD), FXN42-210 (19 kD), and FXN81-210 (15 kD) levels, before and after treatment, were detected by western blot using a primary anti-HA antibody.

## **Chapter 4: G130V Alleviates Mitochondria Dysfunction**

### **4.1 Abstract**

GAA trinucleotide repeats within intron 1 of the Frataxin (*FXN*) gene cause decreased levels of protein and the slowly progressive, early onset Friedreich ataxia. In typical FRDA, disease progression and age of onset correlates with the length of the shortest GAA expansion. 2-3% of FRDA patients carry a GAA expansion on one *FXN* allele, and a missense mutation on the other, and their *FXN* levels are generally lower than typical FRDA patients. This would suggest that such patients have a very severe phenotype; however, these patients can have a mild or severe clinical severity. FRDA patients with the G130V mutation have significantly lower occurrence of cardiomyopathy, scoliosis, and diabetes, and they surpass other point mutation-carrying subjects on composite performance measures accounting for disease duration.

The mechanism by which G130V results in a milder FRDA phenotype is unknown. In this chapter multiple features of mitochondrial function associated with severe typical FRDA phenotype including enzymatic activity, energy metabolism, fusion and ultrastructure were investigated, and compared to that of patients with milder phenotype, carrying the G130V *FXN* missense mutation. Overall, primary fibroblasts from G130V patients appear to have improved mitochondrial function compared to typical FRDA patients, thus providing a rationale linking G130V functional capacity with milder phenotype.



## 4.2 Introduction

Usually presenting in the first two decades of life, Friedreich ataxia (FRDA) causes slowly progressive ataxia, with dysarthria, spasticity in the lower limbs, scoliosis, absence of lower limb reflexes, and loss of position and vibration sense.<sup>9,22,79</sup> At present, there is no cure or effective treatment. FRDA is a recessive neurodegenerative disease, caused by decreased levels of the mitochondrial protein frataxin (FXN) resulting from trinucleotide repeat expansions within intron 1 of the *FXN* gene. In typical FRDA, the length of the shortest GAA expansion correlates with disease severity; longer GAA expansions result in earlier onset and a faster progression.<sup>41,44,86</sup> 2-3% of FRDA patients carry a GAA expansion on one *FXN* allele, and a missense mutation on the other, and their FXN levels are generally lower than typical FRDA patients. The low FXN levels suggest patients should have very severe phenotype. However, the phenotype cannot be predicted based on FXN levels alone; as these patients can have a mild or severe clinical course<sup>45</sup> creating a unique platform to understand clinical and genetic heterogeneity.

In a large cohort of FRDA subjects, those with the G130V mutation have significantly lower levels of cardiomyopathy, scoliosis, and diabetes, and they perform better on composite performance measures than other point mutation-carrying subjects accounting for disease duration. Thus, they retain greater neurological function and decreased disease severity at a similar length of disease duration.<sup>7,19,34,36,37,45,49,82,83,90,125</sup> G130V does not impair FXN localization to mitochondria, but decreases mature FXN<sup>81-210</sup> levels, and is mostly present as the FXN<sup>42-210</sup> intermediate form. Our hypothesis is

that the G130V FXN<sup>42-210</sup> intermediate form has sufficient functional capacity to carry out the role of mature FXN<sup>81-210</sup> for mitochondria function.

Many studies have implicated a role for FXN in iron metabolism, storage and iron-sulfur (Fe-S) cluster biogenesis<sup>23,30,38,60,68,71,80,94,95,110,123</sup>. A conserved primary Fe<sup>2+</sup> binding site, with a dissociation constant within the micromolar range (3–55  $\mu$ M), involves residues of the acidic ridge localized within the first alpha helix<sup>32,81,87,123</sup>. In addition to Fe binding, FXN has been reported to interact with mitochondrial aconitase, ferrochelatase and proteins of the mitochondrial Fe-S cluster machinery.<sup>6,15,50,124</sup> Fe is essential for metabolic processes including oxygen transport, electron transport, DNA synthesis, redox/non-redox reactions and other cell functions.<sup>42,75</sup> In the central nervous system (CNS) and brain, where energy requirements are high, ATP is in high demand for synaptic transmission and distant axoplasmic transport, all of which involve Fe-S enzymes of oxidative metabolism.<sup>31</sup>

Fe-S containing proteins play a crucial role in cellular respiration and ATP production; therefore decreased activity has significant effects on mitochondria function.<sup>15,30</sup> FXN's role in Fe-S cluster biogenesis makes it almost essential for enzymatic activity of Fe-S containing aconitase and respiratory chain complexes. Aconitase, unlike other Fe-S containing proteins, requires Fe-S clusters for activation and conversion of citrate to isocitrate for Krebs cycle metabolism. Consequently, decreased FXN results in decreased aconitase activity, both in cell culture models and *in vivo*, and in heart tissues and biopsies of FRDA patients.<sup>65,70,85,97,102,119</sup> Activities of Fe-S containing proteins of the electron transport chain are also decreased in endomyocardial biopsies of FRDA patients (Complexes I, II, and III),<sup>102</sup> Primary FRDA patient fibroblasts (Complexes I and II),<sup>77</sup> and FRDA mouse models (Complexes I, II, and IV).<sup>33,76</sup>

Mitochondrial iron accumulation is a hallmark of Fe-S deficiency. Friedreich ataxia patients demonstrate iron deposits in cardiomyocytes,<sup>65,70,85</sup> iron metabolism dysregulation in heart autopsies,<sup>70,102</sup> mitochondrial iron overload<sup>85</sup> and deficiency of Fe-S containing enzymes in the CNS.<sup>65</sup> Although its role in disease pathophysiology is uncertain, increased iron within mitochondria could lead to oxidative stress and associated damage of dorsal root ganglion and spinal sensory neurons.<sup>11,23</sup>

Ferritin, a cytosolic protein, binds and stores intracellular iron to prevent the formation of reactive oxygen species (ROS). Ferritin expression is induced by excess iron and has been found at increased levels in some neurodegenerative diseases.<sup>21,35</sup> Mitochondria require iron for heme and Fe-S cluster synthesis, but also generate large amounts of hydrogen peroxide as by-products of respiratory activity.<sup>103</sup> Mitochondrial ferritin (FtMt) is a nuclear-encoded iron-sequestering protein that specifically localizes in mitochondria. FtMt expression can reduce ROS levels, increase ATP levels and the activity of mitochondrial Fe-S enzymes, positively effect cell viability, reduce cytosolic and mitochondrial labile iron pools, rescue respiratory deficiency, reduce mitochondrial iron accumulation, increase resistance to oxidants and protect cells from mitochondrial DNA damage.<sup>20,21,89</sup> In FRDA patient fibroblasts, FtMt expression prevented the formation of ROS and partially rescued the impaired activity of mitochondrial Fe-S enzymes, caused by frataxin deficiency, suggesting FtMt involvement in controlling ROS formation through mitochondrial iron regulation. Histological analysis of FRDA patient samples suggested the role of FtMt in the formation of iron-rich structures,<sup>85</sup> and increased mitoferritin-2 mRNA has been observed in FRDA MCK mice.<sup>59</sup>

In this chapter, I investigate multiple features of mitochondrial dysfunction associated with severe, FRDA phenotype including: FtMt levels, mitochondrial aconitase

activity, Krebs cycle metabolic activity, and mitochondrial ultrastructure. Using primary FRDA fibroblasts, we compared typical FRDA patients with G130V patients to understand molecular mechanisms that may underlie milder phenotype in G130V patients.

## **4.3 Materials and Methods**

### *4.3.1 Immunostaining*

Primary fibroblasts from Control, Typical FRDA, and FRDA patients with G130V mutation were fixed with 4% paraformaldehyde followed by treatment with blocking buffer containing 5% normal goat serum, 3% Triton X-100, and 1% BSA. Primary antibody to the mitochondrial ferritin epitope was added at a 1:100 dilution overnight. Alexa Fluor 488 secondary antibody was added at a dilution of 1:100 and cells were imaged by confocal microscopy.

### *4.3.2 Transfection for Live Imaging*

Primary fibroblasts from Control, Typical FRDA, and FRDA patients with G130V mutation were grown on coverslips and co-transfected via Lipofectamine 2000 reagent with mito-DsRed2 and mito-PAGFP, 1ug each. Twenty four hours after transfection, DsRed2 immunofluorescence was used to select single mitochondria regions of interest, and UV 405 nm laser was used to activate mito-PAGFP for live imaging by confocal microscopy with 5 seconds activation and 2 min time frame.

### *4.3.3 Aconitase Activity*

Mitochondria were isolated from primary Control, typical FRDA, and G130V patient fibroblasts. Aconitase activity was measured using the Aconitase Activity Assay Kit (Sigma MAK051) and activity in typical FRDA and G130V fibroblasts was normalized to control.

#### *4.3.4 Electron Microscopy*

Control, typical FRDA, and G130V primary fibroblasts were washed with 1X PBS, scraped from 10cm plates and gently centrifuged at 23 x *g*. The resulting pellet was fixed with Paraformaldehyde/ Glutaraldehyde solution. Cells were embedded and sectioned in 1 micron sections and images were collected at 75,000x.

#### *4.3.5 Isotope Labeling*

Primary fibroblasts from Control, Typical FRDA, and FRDA patients with G130V mutation were treated with 5mM [<sup>13</sup>C<sub>6</sub>]-Glucose for 3 hours. Cells were collected and gently centrifuged at 23 x *g*. The resulting pellet was suspended in 10% TCA, and prepared for LC-MS using solid phase extraction cleanup.

## 4.4. Results

### *4.4.1 Decreased Mitochondrial Ferritin, Associated with Iron Overload in Typical FRDA, is Absent in G130V Patient Fibroblasts*

I first investigated mitochondrial ferritin (FtMt) levels, observed by Immunohistochemistry, to compare patients with G130V with typical FRDA patients and examine differences that may underlie phenotype severity. Decreased FtMt immunoreactivity, compared to control, was present in typical FRDA patient fibroblasts, as expected, but little to no change, compared to controls, was found in FRDA G130V patient fibroblasts (Figure 4.1). This suggests the G130V mutation has the ability to handle iron in a way that decreases or prevents mitochondria iron overload, thereby contributing to milder phenotype.

### *4.4.2 Increased Mitochondrial Aconitase Activity in G130V FRDA Patient Fibroblasts Compared to Typical FRDA*

I next compared mitochondrial aconitase activity in fibroblasts from control, typical FRDA patients, and FRDA patients with G130V. Mitochondrial aconitase activity is significantly decreased in FRDA fibroblasts and significantly increased in FRDA patients with G130V, compared to typical FRDA patients, and not significantly different compared to controls (Figure 4.2). As FXN<sup>G130V</sup> is present predominantly as the FXN<sup>42-210</sup> intermediate form, this supports functional capacity of FXN<sup>42-210</sup> with G130V mutation to participate in Fe-s cluster biogenesis in order to facilitate aconitase activity, compared to typical FRDA patients.

#### *4.4.3 Increased TCA Metabolic Activity in G130V FRDA Patient Fibroblasts Compared to Typical FRDA*

Friedrich ataxia patients have dysregulated glucose metabolism leading to increased palmitate-derived acyl-CoA thioesters.<sup>5,121</sup> To further examine and compare downstream mechanisms of mitochondria metabolism in control, typical FRDA, and G130V patient fibroblasts, I utilized LC-MS-based isotopologue analysis to measure incorporation of <sup>13</sup>C-labeled carbon from Glucose to Succinyl Co A as a measure of metabolic flux. Consistent with aconitase activity, Krebs cycle metabolic flux is significantly decreased in FRDA fibroblasts compared to controls, while G130V fibroblasts had increased activity compared to typical FRDA but decreased activity compared to controls (Figure 4.3). This suggests that the hypothesized functional capacity of G130V FXN<sup>42-210</sup> to participate in Fe-S cluster biogenesis has downstream effects on both aconitase and Krebs cycle activity as possible contributors to overall improved mitochondria function and milder phenotypes, compared to typical FRDA.

#### *4.4.4 G130V Patients Have Retained Mitochondrial Structure Compared to Typical FRDA Patients*

I further investigated if mitochondria dysfunction at the molecular level was consistent with changes in mitochondrial ultrastructure by utilizing electron microscopy to visualize mitochondrial ultrastructure in order to compare control, typical FRDA, and G130V patient fibroblasts. Disrupted cristae formation and a lack of double membrane structures was observed in typical FRDA patient fibroblasts, but maintained in G130V patient fibroblasts (Figure 4.4A). A difference in glycogen content was also observed. Glycogen levels in typical FRDA patient fibroblasts were significantly decreased compared to both control and G130V, while glycogen content in G130V fibroblasts was



significantly increased compared to both control and typical FRDA fibroblasts (Figure 4.4B). This is consistent with evidence of dysregulated glucose metabolism present in typical FRDA patients, and supports the improved Krebs cycle metabolic flux in G130V fibroblast compared to typical FRDA fibroblasts.

#### *4.4.5 Mitochondrial Fusion is Disrupted in Typical FRDA Patient Fibroblasts, but Preserved in G130V*

Mitochondrial fusion and fission are necessary events for maintaining mitochondria under metabolic or environmental stress. I examined these events in both a fixed-steady state and under dynamic real-time conditions. FRDA patient fibroblasts, both typical and G130V, exhibit a pattern of mitochondrial fragmentation while control fibroblasts maintain linear networks of mitochondria in a fixed-steady state (Figure 4.5). However, while mitochondrial fragmentation is present in both typical and G130V patient fibroblasts, real-time mitochondria fusion is impaired in typical FRDA patient fibroblasts, but maintained in G130V patient fibroblasts (Figure 4.6). This suggests a possible role for FXN G130V at the mitochondrial membrane to facilitate fusion and mitochondrial maintenance as a contributor to milder phenotype.

## 4.5 Discussion

In this chapter mitochondrial functions associated with severe phenotype in typical FRDA were compared to that of patients with milder phenotype, carrying the G130V FXN missense mutation. Primary fibroblasts from G130V patients have increased FtMt immunoreactivity, mitochondrial aconitase activity and Krebs cycle metabolic activity compared to typical FRDA primary fibroblasts. They also have retained mitochondrial ultrastructure and preserved mitochondrial fusion, both of which were disrupted in typical FRDA fibroblasts. Decreased FXN<sup>81-210</sup> levels primarily cause disease, but levels of this form of frataxin alone are not enough to predict disease severity in heterozygous patients with point mutations, as patients with FXN<sup>G130V</sup> have less FXN<sup>81-210</sup> levels than typical FRDA patients. Wild Type FXN<sup>42-210</sup> has functional capacity in participating in Fe-S cluster biogenesis *in vitro*, and the present study suggests that this FXN G130V form has sufficient functional capacity to retain FtMt immunoreactivity and mitochondrial aconitase activity, glucose metabolic flux through the Krebs cycle, mitochondrial ultrastructure, and preserve mitochondrial fusion, all of which was decreased or impaired in typical FRDA patient fibroblasts.

There is greater systemic iron deficiency in typical FRDA patients<sup>121</sup>, compared to G130V patients, as measured by serum ferritin levels. FXN deficiency leads to Fe-S cluster biogenesis deficiency, further leading to mitochondrial iron overload. It has been suggested that the decreased levels of FXN and increased iron within mitochondria lead to oxidative stress and associated damage of dorsal root ganglion and spinal sensory neurons.<sup>23</sup> The protective effects of FtMt, when overexpressed in FXN-deficient cells, included decreased mitochondrial iron overload, preserved mitochondrial DNA integrity, and increased resistance on stress.<sup>20</sup> The observed decrease in FtMt immunoreactivity

in typical FRDA fibroblasts is indicative of mitochondrial iron overload, however immunoreactivity in G130V patients fibroblasts was comparable to control suggesting the G130V mutation provides FXN the ability to handle iron in a way that decreases or prevents mitochondrial iron overload.

FXN plays a role in Fe-S cluster biogenesis, and aconitase is an Fe-S requiring enzyme that participates in Krebs cycle isomerization of isocitrate to citrate. Consequently, FXN deficiency leads to decreased activity of Fe-S containing enzymes. Decreased aconitase activity has been demonstrated in FRDA patient samples but has not been demonstrated in patients with G130V, or other missense mutations. The wild type FXN<sup>42-210</sup> intermediate form participates in Fe-S cluster biogenesis. The decreased level of mitochondrial dysfunction in G130V primary fibroblasts indirectly confirms the functionality of FXN<sup>42-210</sup>, and provides a functional rationale linking the G130V mutation to a milder phenotype. G130V appears to offer additional functional capacity in the FXN<sup>42-210</sup> form that is otherwise not present to typical FRDA patients. The increased aconitase activity, glucose metabolic flux through Krebs cycle, and mitochondrial fusion all support functional capacity of FXN<sup>42-210</sup> with G130V mutation to participate in Fe-s cluster biogenesis and functional capacity at the mitochondrial membrane, leading to healthier mitochondria and improved cell vitality, further contributing to milder phenotype in these patients.

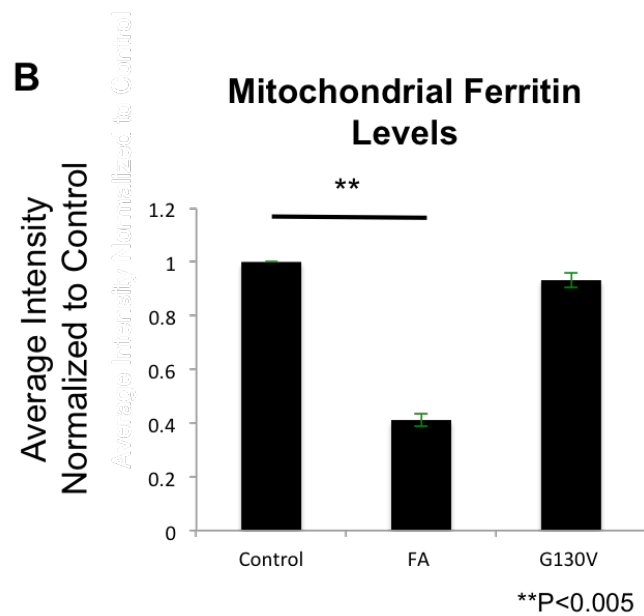
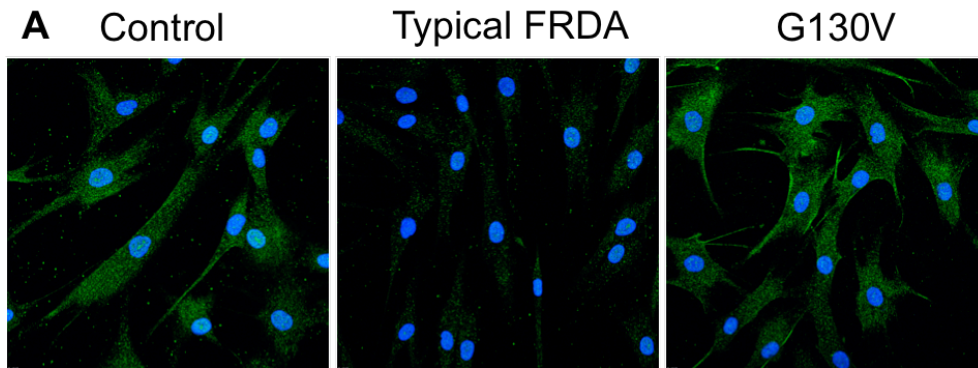


Figure 4.1 Decreased mitochondrial ferritin in as absent in G130V patient fibroblasts. Mitochondrial ferritin levels in primary human fibroblasts from control (CTRL), FRDA, and G130V patients. **A.** Confocal microscopy images of patient fibroblasts (CTRL, FRDA, and G130V) that were fixed and stained using primary anti-mitochondrial ferritin antibody and secondary Alexa Fluor 488 antibody. DAPI was also used as a nuclear stain. **B.** Quantification of mitochondrial ferritin immunoreactivity average intensity. (\*\*) =  $P < 0.05$ .

## Mitochondria Aconitase Activity

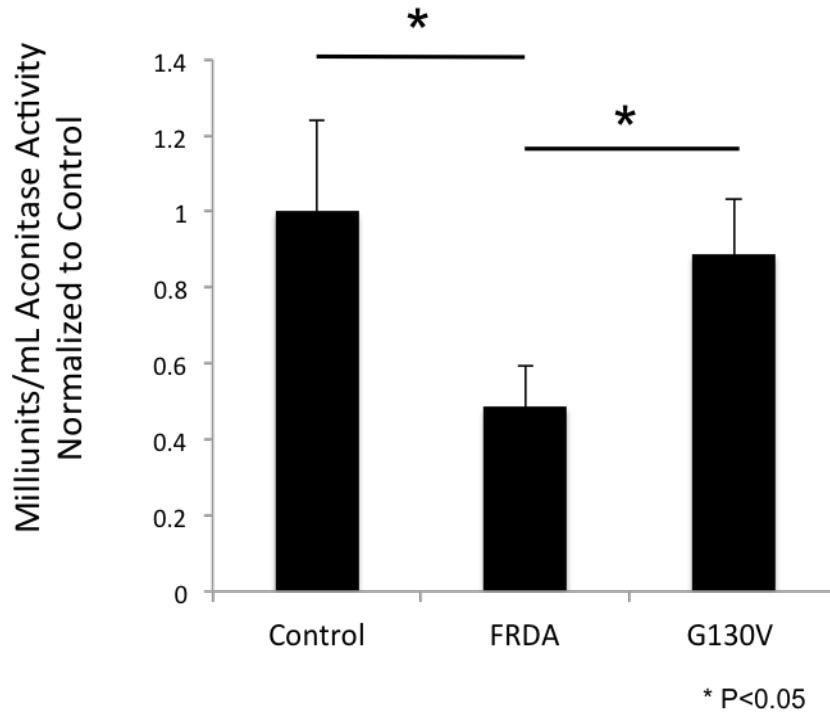


Figure 4.2 Increased Mitochondria Aconitase Activity in G130V FRDA patient fibroblasts. Quantification of mitochondrial aconitase activity (millimunits/mL) from control, FRDA, and G130V fibroblasts, normalized to control. (\*\*\*) = P < 0.0005.

## [<sup>13</sup>C<sub>2</sub>]-Succinyl CoA

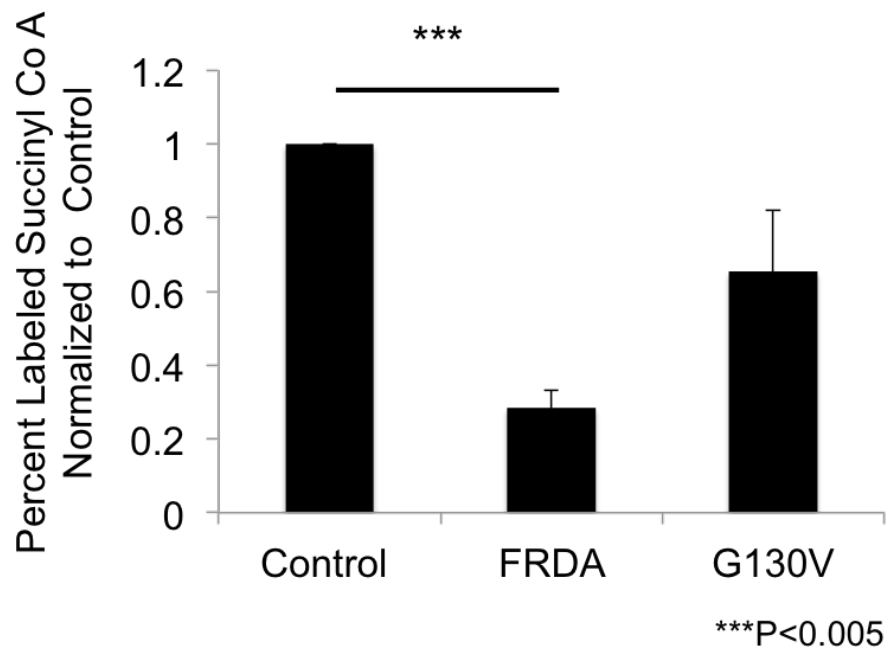


Figure 4.3 Increased TCA metabolic activity in G130V FRDA patient fibroblasts. Quantification of percent labeled [<sup>13</sup>C<sub>2</sub>]-Succinyl Co A following treatment of control, typical FRDA, and G130V fibroblasts with [<sup>13</sup>C<sub>6</sub>]-Glucose for 3 hours, normalized to control. (\*\*\*) = P < 0.0005.

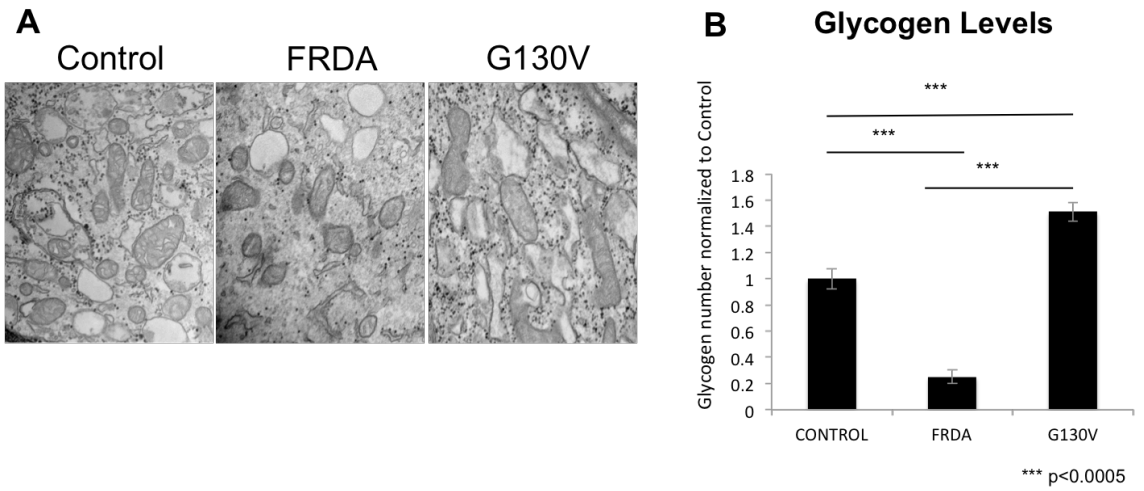


Figure 4.4 G130V patients have retained mitochondria structure and increased glycogen. **A.** Electron microscopy images of control, typical FRDA, and G130V fibroblasts at 75,000x. **B.** Quantification glycogen content normalized to control. (\*\*\*) =  $P < 0.0005$ .

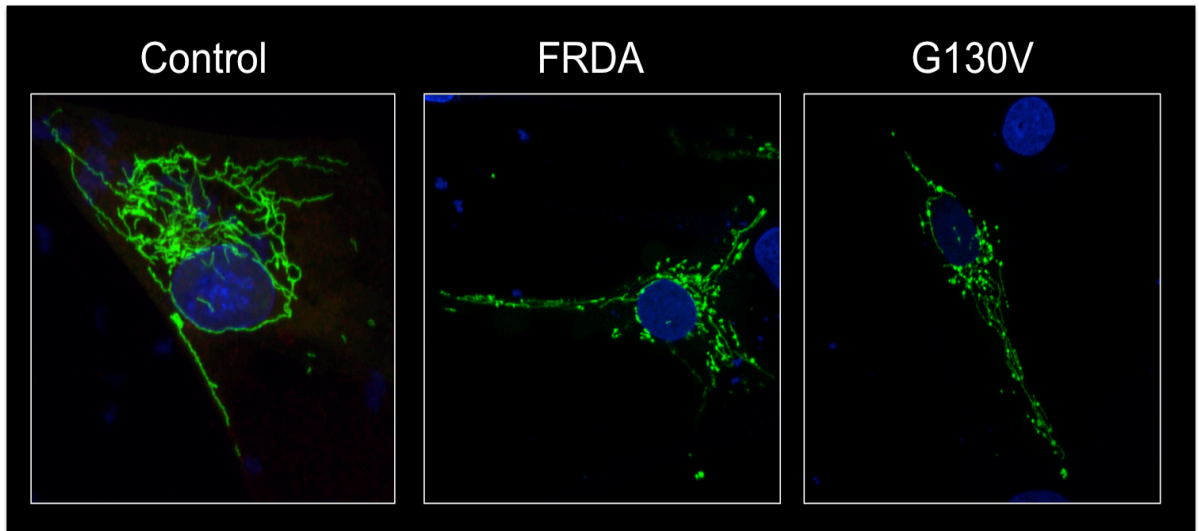


Figure 4.5 Mitochondria fragmentation in FRDA patient fibroblasts. Confocal microscopy images of patient fibroblasts (CTRL, FRDA, and G130V) transfected with mito-GFP and fixed. DAPI was also used as a nuclear stain.



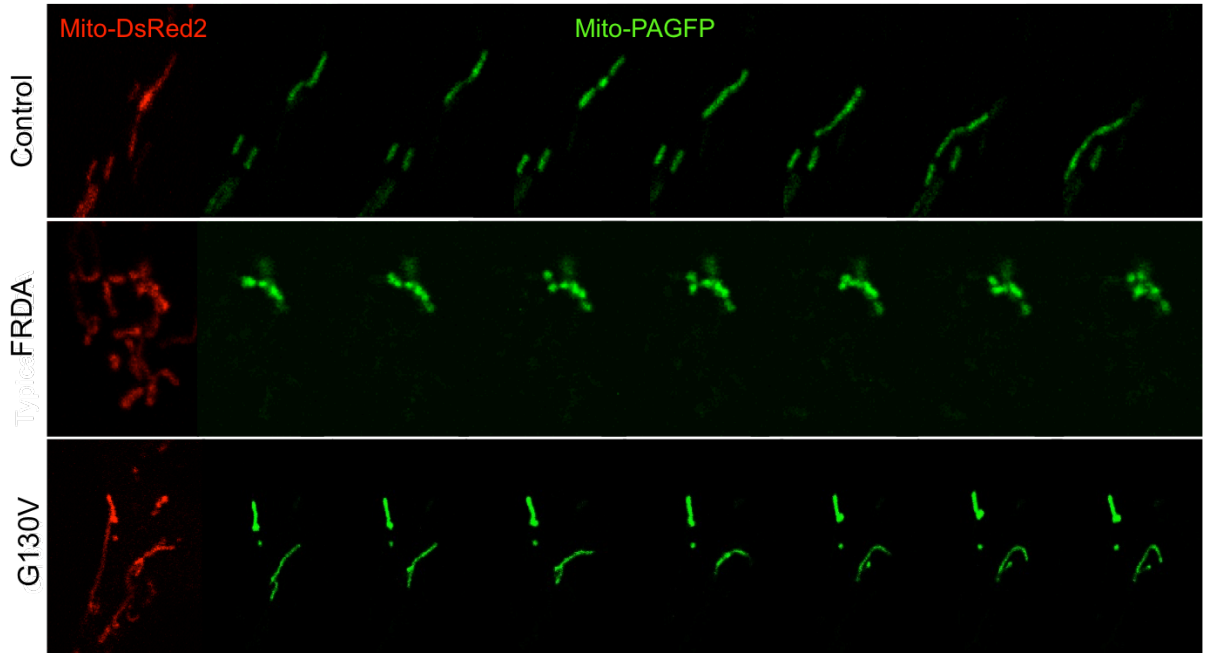
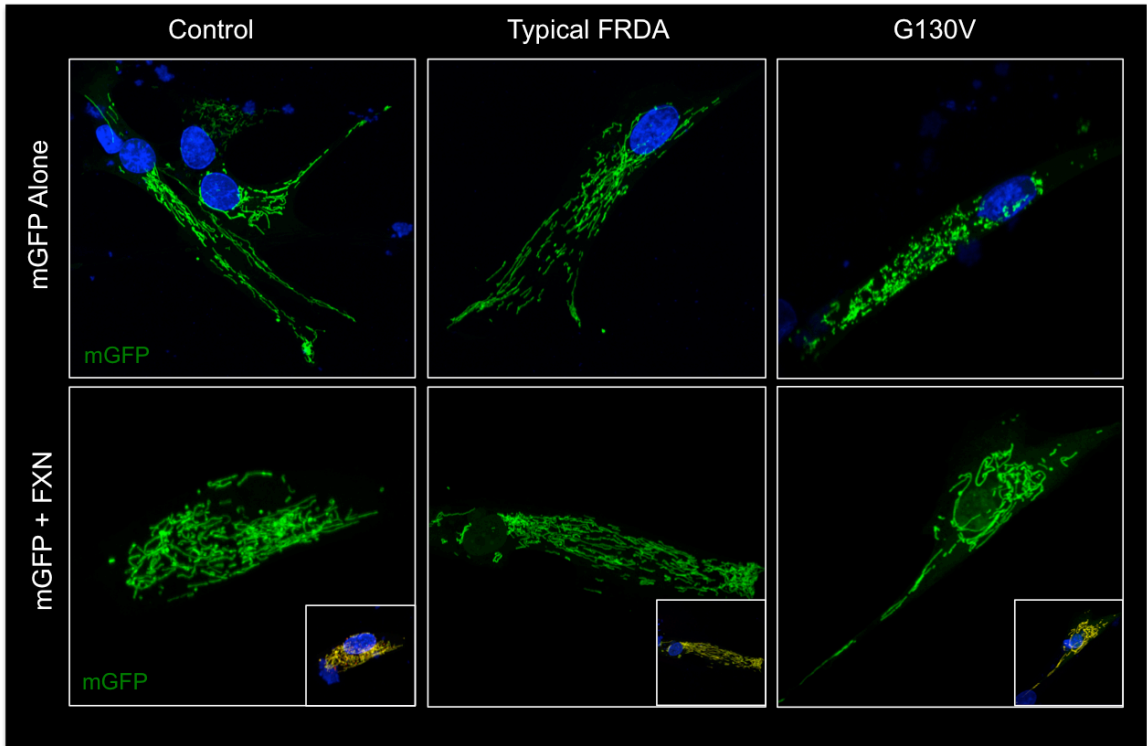


Figure 4.6 Mitochondria fusion is preserved in G130V patient fibroblasts. Time-lapse images of Control, typical FRDA, and G130V fibroblasts co-transfected with mito-DsRed2 and mito-PAGFP, activated for 5 seconds and imaged for 2 minutes.



Supplemental Figure 4.1 Confocal microscopy images of control, typical FRDA, and G230V fibroblasts cotransfected with WT FXN and mitoGFP, fixed, and stained using a primary anti-HA antibody to detect exogenous FXN only and secondary antibody Alexa Fluor 568. DAPI was also used as a nuclear stain.

## **Chapter 5: Conclusions and Future Directions**

### **5.1 Conclusions**

In this thesis, I sought to understand the mechanism by which disease-associated missense mutation lead to mutation-selective phenotypes in FRDA by investigating the effects of FRDA-associated missense mutations on FXN import into the mitochondria and FXN processing, examining multiple features of mitochondria function associated with severe typical FRDA phenotype and compared it to that of patients with milder phenotype carrying the G130V FXN missense mutation.

The effects of FRDA-associated missense mutations on FXN import into the mitochondria were first investigated by co-transfection of FXN variants containing a C-terminal HA tag and mito-GFP in HEK 293 cells. With the exception of L106S, a protein folding mutation that produces no protein, all variants: R165C, W155R, I154F, G130V, and G137V co-localized with mito-GFP with a Pearson's correlation coefficient greater than 0.98 and retained their mitochondria localization. FRDA patients carrying a missense mutation generally have lower mature FXN<sup>81-210</sup> levels than typical FRDA patients. This is consistent with the decreased immunoreactivity in I154F, G130V, and G137V by immunocytochemistry and western blot. To further investigate the decreased FXN<sup>81-210</sup> levels of particular FXN-mutant proteins, subcellular fractionation and separation of the soluble and insoluble mitochondrial pellet was performed. R165C or W155R resulted in FXN<sup>81-210</sup> levels comparable to WT, while transfection of I154F or G130V produced lower levels of FXN<sup>81-210</sup> and increased levels of FXN<sup>42-210</sup>, suggesting these FXN variants are not processed readily from FXN<sup>42-210</sup> to the FXN<sup>81-210</sup> form.

Increased ratios of insoluble to soluble FXN<sup>42-210</sup> were observed, suggesting these proteins remain associated with the insoluble inner mitochondrial membrane rather than being released into the soluble portion of the mitochondrion. To examine the mechanism by which I154F and G130V impair FXN processing, co-immunoprecipitation was performed to study the strength of the interaction between FXN and MPP. FXN<sup>42-210</sup> forms of I154F and G130V are more readily co-immunoprecipitated by anti-MPP than the FXN<sup>42-210</sup> form of WT, R165C, and W155R proteins, suggesting stronger attachment between these variants and MPP. I next modeled the approach of traditional therapies to increase FXN levels using the proteasome inhibitor MG132. While I154F and G130V FXN<sup>1-210</sup> and FXN<sup>42-210</sup> levels increased, MG132 treatment did not increase FXN<sup>81-210</sup> levels suggesting that increasing FXN<sup>81-210</sup> cannot be achieved with simple overexpression of precursor FXN. Conclusively, the significance of these findings was analyzed in patient-derived cells including Controls, Typical FRDA, and G130V patients, and the processing of native FXN was examined by western blot. Indeed, the ratio of FXN<sup>42-210</sup> to FXN<sup>81-210</sup> was increased in primary FRDA G130V patient fibroblasts, and large globular structures, consistent with the increased insoluble FXN<sup>42-210</sup> form detected by western blot and overexpression studies, was observed. We then sought to establish whether patients carrying missense point mutations displayed distinct clinical abnormalities that could be related to the altered processing observed *in vitro*. Patients carrying G130V mutations have significantly lower occurrence of cardiomyopathy, scoliosis, and diabetes, the most severe components of the disease, compared to patients with other mutations, and patients with an I154F mutation fell between the phenotypic severity of G130V and other point mutations. We hypothesize that the incompletely processed FXN<sup>42-210</sup> carries some residual activity. This form is located in the mitochondria, and others suggest that FXN<sup>42-210</sup> can perform Fe-S cluster synthesis

as well as participate in cysteine desulfurase activity as efficiently as FXN<sup>81-210</sup>. Thus, the higher levels of FXN<sup>42-210</sup> associated with G130V and I154F could lead to the milder phenotype if this intermediate form is functional.

In addition to these disease-associated mutations, a patient who carries a novel W168R missense mutation, and 1133 expanded GAA repeats on the opposite allele, with extremely low levels of mature FXN<sup>81-210</sup> levels and an especially severe phenotype was presented. Based on the amino acid position 168, it is unlikely to alter FXN levels by misfolding. In order to understand the mechanism by which W168R contributes to severe phenotype, FXN import into the mitochondria, FXN processing, as well as FXN interaction with MPP was investigated. W168R is expressed predominantly as the intermediate FXN<sup>42-210</sup> form, with little to no expression of the mature FXN<sup>81-210</sup> form consistent with patient samples, its localization to the mitochondria is not impaired, and modeling traditional therapies to increase FXN<sup>1-210</sup> levels does not increase mature FXN levels. The G130V mutation, associated with milder phenotype, is also expressed predominantly as the intermediate FXN<sup>42-210</sup> form, with very low mature FXN<sup>81-210</sup> form. However, we believe the phenotypic differences likely to reflect mutation-specific functional differences leading to mutation-specific phenotypes.

The mechanism by which G130V results in a milder FRDA phenotype is unknown, thus I investigated multiple features of mitochondria function associated with severe, typical FRDA phenotype including enzymatic activity, energy metabolism, fusion and ultrastructure, and compared it to that of patients with milder phenotype, carrying the G130V FXN missense mutation. Mitochondrial ferritin levels were first examined by Immunohistochemistry. As expected, decreased mitochondria ferritin immunoreactivity was present in typical FRDA patient fibroblasts, but little to no change, compared to

controls, was found in G130V patient fibroblasts, suggesting the functional capacity of G130V to handle iron in a way that decreases or prevents mitochondria iron overload. Next, mitochondrial aconitase activity was compared with significantly decreased activity in typical FRDA fibroblasts, and significantly increased activity in G130V fibroblasts compared to typical FRDA patients and no significant difference compared to controls. Downstream mechanisms of mitochondria metabolism were then examined by LC-MS-based isotopologue analysis to measure incorporation of  $^{13}\text{C}$ -labeled carbon from Glucose to Succinyl Co A as a measure of metabolic flux. Consistent with aconitase activity, Krebs cycle metabolic flux was significantly decreased in FRDA fibroblasts and significantly increased in G130V patients compared to typical FRDA patients and no significant difference compared to controls. This supports the hypothesized functional capacity of G130V FXN<sup>42-210</sup> to participate in Fe-S cluster biogenesis and suggest G130V has downstream effects on both aconitase and Krebs cycle activity as possible contributors to overall improved mitochondria function and milder phenotypes, compared to typical FRDA. Subsequently, I investigated if the disrupted molecular mechanisms were consistent with disrupted mitochondria structure by utilizing electron microscopy and real-time imaging. Disrupted cristae formation and a lack of double membrane structures was observed in typical FRDA patient fibroblasts, but maintained in G130V patient fibroblasts. Decreased glycogen content was also observed in typical FRDA fibroblasts consistent with evidence of dysregulated glucose metabolism in FRDA patients. Mitochondrial fusion was examined under fixed-steady state and dynamic real-time conditions. FXN deficiency leads to mitochondria fragmentation in typical FRDA and G130V fibroblasts, while control fibroblasts maintained linear networks of mitochondria in a fixed-steady state. However, real-time mitochondria fusion is impaired in typical FRDA patient fibroblasts, but maintained in G130V patient fibroblasts, suggesting a possible

role for G130V at the mitochondria membrane to facilitate fusion and mitochondria maintenance as a contributor to milder phenotype. Taken together, fibroblasts from G130V patients overall appear to have improved mitochondria function compared to typical FRDA patients, thus providing a rationale linking G130V functional capacity with milder phenotype.

## 5.2 Future directions

In this thesis I have identified mechanisms that underlie mutation-selective phenotypes in FRDA patients with missense mutations. G130V, I154F, and W168R, impair processing from intermediate FXN<sup>42-210</sup> to mature FXN<sup>81-210</sup> form, and increased levels of the G130V FXN<sup>42-210</sup> is associated with milder phenotypes, not only in overexpression studies using mammalian systems, but also in primary fibroblasts from FRDA patients. While others suggest that WT FXN<sup>42-210</sup> can perform Fe-S cluster synthesis as well as participate in cysteine desulfurase activity as efficiently as WT, this is true also for the FXN<sup>42-210</sup> form of W155R, a characterized dysfunctional mutation. The W155R mutation does not impair processing and is predominantly expressed as mature FXN<sup>81-210</sup>, therefore the severe phenotype could be associated with the dysfunctional FXN<sup>81-210</sup> in addition to GAA expansion on the other FXN allele. We believe the incompletely processed FXN<sup>42-210</sup> of G130V carries some residual activity, thus higher levels of FXN<sup>42-210</sup> associated could lead to the mild phenotype of patients if this intermediate form is functional. Further experiments examining the functional capacity of the endogenous FXN<sup>42-210</sup> form missense mutation may help clarify these possibilities. First, *in vitro* studies using site-directed mutagenesis of FXN<sup>42-210</sup> constructs can be used to establish if G130V and W168R can perform Fe-S cluster synthesis as well as participate in cysteine desulfurase activity. If there were functional differences that correlated with disease-associated phenotypes it would provide a functional mechanism by which these mutations lead to the mutation-selective phenotypes.

I also showed that traditional therapies to increase precursor FXN<sup>1-210</sup> levels would not increase mature FXN<sup>81-210</sup> levels. Patients with missense mutations carry the mutation on one FXN allele and GAA expansion on the other. If this approach increased



FXN<sup>81-210</sup> levels of the GAA expanded FXN allele only by 20% and it was sufficient to delay disease progression, then it would still be beneficial if the patient does not carry a missense mutation characterized as dysfunctional. Furthermore, increasing G130V FXN<sup>1-210</sup> resulted in increased FXN<sup>42-210</sup>. If the G130V intermediate FXN<sup>42-210</sup> form were functional, it would also be an additional beneficial to the patients.

Patients with the G130V mutation have significantly lower occurrence of cardiomyopathy, scoliosis, and diabetes, and they surpass other point mutation-carrying subjects on composite performance measures accounting for disease duration. Finally, multiple features of mitochondria dysfunction associated with severe FRDA phenotype including: mitochondria ferritin levels, mitochondria aconitase activity, Krebs cycle metabolic activity, and mitochondria ultrastructure using primary FRDA fibroblasts were investigated. By comparing typical FRDA patients with G130V patients I sought to assess molecular mechanisms that may underlie milder phenotype in G130V patients.

Many studies have implicated a role for FXN in iron metabolism, storage and iron-sulfur cluster biogenesis. Mitochondrial iron accumulation is a hallmark of Fe-S deficiency. Although its role in disease pathophysiology is uncertain, increased iron within mitochondria could have downstream effects leading to oxidative stress and associated damage of dorsal root ganglion and spinal sensory neurons. Mitochondria ferritin expression can reduce reactive oxygen species (ROS) levels, increase ATP levels and the activity of mitochondrial Fe-S enzymes, positively effect cell viability, reduce cytosolic and mitochondrial labile iron pools, rescue respiratory deficiency, reduce mitochondrial iron accumulation, increase resistance to oxidants and protect cells from mitochondrial DNA damage. Decreased mitochondrial ferritin was observed, which is associated with iron overload in typical FRDA fibroblasts. G130V patient fibroblasts

maintained mitochondrial ferritin levels comparable to controls, suggesting that G130V mutation has the ability to handle iron in a way that decreases or prevents mitochondria iron overload. To examine this further, a colorimetric assay could be used to measure iron levels from whole cell lysates and isolated mitochondria from patient fibroblasts. An acidic buffer could be used to release iron in order to bind a chromagen resulting in a colorimetric (593 nm) product, proportional to the iron present. A number of compounds currently in the FRDA research pipeline are designed to decrease iron toxicity. This approach could also be used to compare the effectiveness of these drugs in typical FRDA and G130V patients, further supporting the hypothesized functional capacity of G130V FXN<sup>42-210</sup> to participate in Fe-S cluster synthesis and explain the overall improved mitochondria function as a result of increased FXN function.

FXN has also been implicated in energy metabolism and ATP production. The increased mitochondria aconitase enzymatic activity and Krebs cycle metabolic activity in G130V fibroblasts further supports the hypothesized functional capacity of FXN<sup>42-210</sup> with G130V mutation to participate in Fe-S cluster biogenesis and lead to downstream effects on metabolism and milder phenotype compared to typical FRDA. The impaired mitochondria fusion under normal conditions in typical FRDA fibroblasts suggests FXN deficiency leads to downstream effects functions both within the mitochondria and at the membrane. Mitochondria number and electron chain complex activity is decreased as a result of FXN deficiency in typical FRDA. FXN overexpression reverses mitochondria fragmentation in both typical FRDA and G130V fibroblasts at steady state conditions (Supplemental Figure 4.1). The question remains if increasing FXN levels will also improve mitochondria enzymatic and metabolic activity, or if FRDA-associated FXN deficiency over time leads to irreversible dysfunction. In order to assess if FXN has a direct role in reversing fragmentation associated with FRDA pathology, fibroblasts could

be treated with mitochondria fission inhibitor, such as DRP1 inhibitor Mdivi-1, to see if the reversed fragmentation is consistent. Following fragmentation reversal mitochondria aconitase activity and [13C]-isotopologue analysis for Krebs cycle metabolic activity could be measured to assess any improvement compared to typical FRDA baseline as well as control and G130V. If there were no improvement that would suggest that other therapies with mitochondria targets, such as PGC1 alpha up-regulators for mitochondria biogenesis or Nrf2 activators, might be required. FXN deficiency is also associated with decreased glucose incorporation and increased palmitate-derived acyl-CoA thioesters formation in FRDA platelets compared with controls. Fibroblasts are limited as a model system for studying metabolism, whereas platelets are metabolically active and analyte-rich, and used for biomarker studies to monitor new therapeutic approaches for the treatment of FRDA. It would be interesting to assess these functional differences Krebs cycle, lipid and fatty acid metabolism pathways in platelets from control, typical FRDA, and G130V patients to assess correlation between metabolism and phenotype.

## References

1. Adinolfi S, Trifuoggi M, Politou AS, et al. A structural approach to understanding the iron-binding properties of phylogenetically different frataxins. *Hum.Mol. Genet.* **11**, 1865–1877 (2002).
2. Al-Mahdawi S, Pinto RM, Varshney D, et al. GAA repeat expansion mutation mouse models of Friedreich ataxia exhibit oxidative stress leading to progressive neuronal and cardiac pathology. *Genomics.* **88**, 580–590 (2006).
3. Al-Mahdawi S, Pinto R, Ismail O, et al. The Friedreich ataxia GAA repeat expansion mutation induces comparable epigenetic changes in human and transgenic mouse brain and heart tissues. *Hum. Mol. Genet.* **17**, 735–746 (2008).
4. Balaban RS, Nemoto S, Finkel T. Mitochondria, oxidants, and aging. *Cell* **120**, 483–495 (2005).
5. Basu SS, Deutsch EC, Schmaier AA, et al. Human platelets as a platform to monitor metabolic biomarkers using stable isotopes and LC-MS. *Bioanalysis.* **5**, 3009-3021 (2013).
6. Bencze KZ, Yoon T, Millan-Pacheco C, et al. Human frataxin: iron and ferrochelatase binding surface. *Chem. Commun.* **14**, 1798–1800 (2007).
7. Bidichandani S, Ashizawa T, Patel P. Atypical Friedreich ataxia caused by compound heterozygosity for a novel missense mutation and the GAA triplet-repeat expansion. *Am J Hum Genet.* **60**, 1251–1256 (1997).
8. Bidichandani SI, Purandare SM, Taylor EE, et al. Somatic sequence variation at the Friedreich ataxia locus includes complete contraction of the expanded GAA triplet repeat, significant length variation in serially passaged lymphoblasts and enhanced mutagenesis in the flanking sequence. *Hum Mol Genet.* **8**, 2425-2436 (1999).
9. Bidichandani S, Delatycki M. Friedreich Ataxia. *Gene Reviews.* (2014)
10. Boddaert N, Le Quan Sang KH, Rötting A, et al. Selective iron chelation in Friedreich ataxia: biologic and clinical implications. *Blood.* **110**, 401–408 (2007).
11. Bradley JL, Blake JC, Chamberlain S, et al. Clinical, biochemical and molecular genetic correlations in Friedreich's ataxia. *Hum Mol Genet.* **9**, 275–282 (2000).

12. Bradley JL, Homayoun S, Hart PE, et al. Role of oxidative damage in Friedreich's ataxia. *Neurochem. Res.* **29**, 561–567 (2004).
13. Branda SS, Cavadini P, Adamec J, et al. Yeast and human frataxin are processed to mature form in two sequential steps by the mitochondrial processing peptidase. *J. Biol. Chem.* **274**, 22763–22769 (1999).
14. Bridwell-Rabb J, Winn AM, Barondeau DP. Structure-function analysis of Friedreich's ataxia mutants reveals determinants of frataxin binding and activation of the Fe-S assembly complex. *Biochemistry.* **50**, 7265–7274 (2011).
15. Bulteau AL, O'neill HA, Kennedy MC, et al. Frataxin acts as an iron chaperone protein to modulate mitochondrial aconitase activity. *Science.* **305**, 242–245 (2004).
16. Busi MV, Maliandi MV, Valdez H, et al. Deficiency of Arabidopsis thaliana frataxin alters activity of mitochondrial Fe–S proteins and induces oxidative stress. *Plant J.* **48**, 873–882 (2006).
17. Calabrese V, Lodi R, Tonon C, et al. Oxidative stress, mitochondrial dysfunction and cellular stress response in Friedreich's ataxia. *J Neurol Sci.* **233**, 145–162 (2005).
18. Calmels N, Seznec H, Villa P, et al. Limitations in a frataxin knockdown cell model for Friedreich ataxia in a high-throughput drug screen. *BMC Neurol* **9**, 46 (2009).
19. Calmels N, Schmucker S, Wattenhofer-Donze M, et al. The first cellular models based on frataxin missense mutations that reproduce spontaneously the defects associated with Friedreich ataxia. *PLoS ONE.* **4**, e6379 (2009).
20. Campanella A, Isaya G, O'Neill HA, et al. The expression of human mitochondrial ferritin rescues respiratory function in frataxin-deficient yeast. *Hum. Mol. Genet.* **13**, 2279–2288 (2004).
21. Campanella A, Rovelli E, Santambrogio P, et al. Mitochondrial ferritin limits oxidative damage regulating mitochondrial iron availability: hypothesis for a protective role in Friedreich ataxia. *Hum Mol Genet.* **18**, 1-11 (2009).

22. Campuzano V, Montermini L, Moltò MD, et al. Friedreich's ataxia: autosomal recessive disease caused by an intronic GAA triplet repeat expansion. *Science*. **271**, 1423–1427 (1996).
23. Campuzano V, Montermini L, Lutz Y, et al. Frataxin is reduced in Friedreich ataxia patients and is associated with mitochondrial membranes. *Hum Mol Genet*. **6**, 1771–1780 (1997).
24. Castaldo I, Pinelli M, Monticelli A, et al. DNA methylation in intron 1 of the frataxin gene is related to GAA repeat length and age of onset in Friedreich ataxia patients. *J. Med. Genet*. **45**, 808–812 (2008).
25. Cavadini P, Adamec J, Taroni F, et al. Two-step processing of human frataxin by mitochondrial processing peptidase. Precursor and intermediate forms are cleaved at different rates. *J. Biol. Chem*. **275**, 41469–41475 (2000).
26. Cavadini P, Gellera C, Patel P, et al. Human frataxin maintains mitochondrial iron homeostasis in *Saccharomyces cerevisiae*. *Hum Mol Genet*. **9**, 2523–2530 (2009).
27. Chantrel-Groussard K, Geromel V, Puccio H, et al. Disabled early recruitment of antioxidant defenses in Friedreich's ataxia. *Hum. Mol. Genet*. **10**, 2061–2067 (2001).
28. Chiueh CC. Iron overload, oxidative stress, and axonal dystrophy in brain disorders. *Pediatr Neurol*. **25**, 138–147 (2001).
29. Clark E, Butler J, Issacs J, et al. Selected missense mutations impair frataxin processing in Friedreich ataxia. *Ann Clin Transl Neurol*. **4**, 575–584 (2017).
30. Colin F, Martelli A, Clemancey M, et al. Mammalian frataxin controls sulfur production and iron entry during de novo Fe<sub>4</sub>S<sub>4</sub> cluster assembly. *J. Am. Chem. Soc*. **135**, 733–740 (2013).
31. Connor JR, Menzies SL, Burdo JR, et al. Iron and iron management proteins in neurobiology. *Pediatr Neurol*. **25**, 118–129 (2001).
32. Cook JD, Bencze KZ, Jankovic AD, et al. Monomeric yeast frataxin is an iron-binding protein. *Biochemistry*. **45**, 7767–7777 (2006).

33. Coppola G, Marmolino D, Lu D, et al. Functional genomic analysis of frataxin deficiency reveals tissue-specific alterations and identifies the PPAR gamma pathway as a therapeutic target in Friedreich's ataxia. *Hum. Mol. Genet.* **18**, 2452-2461 (2009).
34. Cossee M, Durr A, Schmitt M, et al. Friedreich's ataxia: point mutations and clinical presentation of compound heterozygotes. *Ann Neurol.* **45**, 200–206 (1999).
35. Curtis AR, Fey C, Morris CM, et al. Mutation in the gene encoding ferritin light polypeptide causes dominant adult-onset basal ganglia disease. *Nat Genet.* **28**, 350–354 (2001).
36. Delatycki MB, Knight M, Koenig M, et al. G130V, a common FRDA point mutation, appears to have arisen from a common founder. *Hum Genet.* **105**, 343–346 (1999).
37. Delatycki M, Williamson R, Forrest S. Friedreich ataxia: an overview. *J Med Genet.* **37**, 1–8 (2000).
38. Dhe-Paganon S, Shigeta R, Chi Y, et al. Crystal structure of human frataxin. *J Biol Chem.* **275**, 30753–30756 (2000).
39. Di Prospero NA, Baker A, Jeffries N, et al. Neurological effects of high-dose idebenone in patients with Friedreich's ataxia: a randomised, placebo-controlled trial. *Lancet. Neurol.* **6**, 878–886 (2007).
40. Di Prospero N and Fischbeck K. Therapeutics development for triplet repeat expansion diseases. *Nat. Rev. Genet.* **6**, 756–765 (2005).
41. Dürr A, Cossee M, Agid Y, et al. Clinical and genetic abnormalities in patients with Friedreich's ataxia. *N. Engl. J. Med.* **335**, 1169–1175 (1996).
42. Eisenstein R. Iron regulatory proteins and the molecular control of mammalian iron metabolism. *Annu Rev Nutr.* **20**, 627–662 (2000).
43. Emond M, Lepage G, Vanasse M, et al. Increased levels of plasma malondialdehyde in Friedreich ataxia. *Neurology.* **55**, 1752–1753 (2000).
44. Filla A, De Michele G, Cavalcanti F, et al. The relationship between trinucleotide (GAA) repeat length and clinical features in Friedreich ataxia. *Am. J. Hum. Genet.* **59**, 554–560 (1996).

45. Forrest S, Knight M, Delatycki M, et al. The correlation of clinical phenotype in Friedreich ataxia with the site of pointmutations in the FRDA gene. *Neurogenetics*. **1**, 253-257 (1998).
46. Fourquet S, Huang ME, D'Autreaux B, et al. The dual functions of thiol-based peroxidases in H<sub>2</sub>O<sub>2</sub> scavenging and signaling. *Antioxid Redox Signal*. **10**, 1565–1576 (2008).
47. Friedreich N. Ueber degenerative Atrophie der spinalen Hinterstränge. *Virchow's Arch Pathol Anat*. **26**, 433–459 (1863).
48. Galea CA, Huq A, Lockhart PJ, et al. Compound heterozygous FXN mutations and clinical outcome in Friedreich ataxia. *Ann Neurol*. **79**, 485–495 (2016)
49. Gellera C, Castellotti B, Mariotti C, et al. Frataxin gene point mutations in Italian Friedreich ataxia patients. *Neurogenetics*. **8**, 289–299 (2007).
50. Gerber J, Muhlenhoff U, Lill, R. An interaction between frataxin and Isu1/Nfs1 that is crucial for Fe/S cluster synthesis on Isu1. *EMBO Rep*. **4**, 906–911 (2003).
51. Goncalves S, Paupe V, Dassa EP, et al. Deferiprone targets aconitase: implication for Friedreich's ataxia treatment. *BMC Neurol*. **8**, 20 (2008).
52. Gonzalez-Cabo P, Vazquez-Manrique RP, Garcia-Gimeno MA, et al. Frataxin interacts functionally with mitochondrial electron transport chain proteins. *Hum Mol Genet*. **14**, 2091–2098 (2005).
53. Gonzalez-Cabo P and Palau F. Mitochondrial pathophysiology in Friedreich's ataxia. *J Neurochem*. **126**, 53-64 (2013)
54. Gordon D, Shi Q, Dancis A, et al. Maturation of frataxin within mammalian and yeast mitochondria: one-step processing by matrix processing peptidase. *Hum Mol Genet*. **8**, 2255–2262 (1999).
55. Greene E, Mahishi L, Entezam A, et al. Repeat-induced epigenetic changes in intron 1 of the frataxin gene and its consequences in Friedreich ataxia. *Nucleic Acids Res*. **35**, 3383–3390 (2007).



56. Hart PE, Lodi R, Rajagopalan B, et al. Antioxidant treatment of patients with Friedreich ataxia: four-year follow-up. *Arch Neurol.* **62**, 621–626 (2005).
57. Herman D, Jenssen K, Burnett R, et al. Histone deacetylase inhibitors reverse gene silencing in Friedreich's ataxia. *Nat. Chem. Biol.* **2**, 551–558 (2006).
58. Herrero E, Ros J, Belli´ G, et al. Redox control and oxidative stress in yeast cells. *Biochim Biophys Acta.* **1780**, 1217–1235 (2008).
59. Huang ML, Becker EM, Whitnall M, et al. Elucidation of the mechanism of mitochondrial iron loading in Friedreich's ataxia by analysis of a mouse mutant. *Proc.Natl.Acad. Sci.U.S.A.* **106**, 16381–16386 (2009).
60. Huynen MA, Snel B, Bork P, et al. The phylogenetic distribution of frataxin indicates a role in iron-sulfur cluster protein assembly. *Hum.Mol. Genet.* **10**, 2463–2468 (2001).
61. Irazusta V, Cabiscol E, Reverter-Branchat G, et al. Manganese is the link between frataxin and iron–sulfur deficiency in the yeast model of Friedreich ataxia. *J. Biol. Chem.* **281**, 12227–12232 (2006).
62. Jauslin ML, Meier T, Smith RA, et al. Mitochondria-targeted antioxidants protect Friedreich ataxia fibroblasts from endogenous oxidative stress more effectively than untargeted antioxidants. *FASEB J.* **17**, 1972–1974 (2003).
63. Jiralerspong S, Ge B, Hudson TJ, et al. Manganese superoxide dismutase induction by iron is impaired in Friedreich ataxia cells. *FEBS Lett.* **509**, 101–105 (2001).
64. Kakhlon O, Manning H, Breuer W, et al. Cell functions impaired by frataxin deficiency are restored by drugmediated iron relocation. *Blood.* **112**, 5219–5227 (2008).
65. Koeppen AH, Michael SC, Knutson MD, et al. The dentate nucleus in Friedreich's ataxia: the role of iron-responsive proteins. *Acta Neuropathol.* **114**, 163–173 (2007).
66. Koopman WJ, Hink MA, Verkaart S, et al. Partial complex I inhibition decreases mitochondrial motility and increases matrix protein diffusion as revealed by fluorescence correlation spectroscopy. *Biochim Biophys Acta.* **1767**, 940–947 (2007).

67. Koopman WJ, Verkaart S, Visch HJ, et al. Human NADH: ubiquinone oxidoreductase deficiency: radical changes in mitochondrial morphology? *Am J Physiol Cell Physiol.* **293**, 22C-29 (2007)
68. Koutnikova H, Campuzano V, Foury F, et al. Studies of human, mouse and yeast homologues indicate a mitochondrial function for frataxin. *Nat. Genet.* **16**, 345–351 (1997).
69. Koutnikova H, Campuzano V, Koenig M. Maturation of wild-type and mutated frataxin by the mitochondrial processing peptidase. *Hum Mol Genet.* **7**, 1485–1489 (1998).
70. Lamarche JB, Cote M, Lemieux B. The cardiomyopathy of Friedreich's ataxia morphological observations in 3 cases. *Can. J.Neurol.Sci.* **7**, 389–396 (1980).
71. Layer G, Ollagnier-De Choudens S, Sanakis Y, et al. Iron-sulfur cluster biosynthesis: characterization of *Escherichia coli* CYaY as an iron donor for the assembly of [2Fe-2S] clusters in the scaffold IscU. *J. Biol. Chem.* **281**, 16256–16263 (2006).
72. Lazaropoulos M, Dong Y, Clark E, et al. Measurement of frataxin levels in peripheral tissue in Friedreich ataxia: Analysis using repeated measures. *Ann Clin Transl Neurol.* **2**, 831-842 (2015).
73. Li H, Gakh O, Smith DY, et al. Missense mutations linked to Friedreich ataxia have different but synergistic effects on mitochondrial frataxin isoforms. *J Biol Chem.* **6**, 4116–4127 (2013).
74. Li K, Besse E, Ha D, et al. Iron-dependent regulation of frataxin expression: implications for treatment of Friedreich ataxia. *Hum. Mol. Genet.* **17**, 2265–2273 (2008).
75. Lieu P, Heiskala M, Peterson P, et al. The roles of iron in health and disease. *Mol Aspects Med.* **22**, 1–87 (2001).
76. Lin H, Magrane J, Rattelle A, et al. Early cerebellar deficits in mitochondrial biogenesis and respiratory chain complexes in the KIKO mouse model of Friedreich ataxia. *Dis Model Mech.* **10**, 1343–1352 (2017).
77. Lobmayr L, Brooks DG, Wilson RB. Increased IRP1 activity in Friedreich ataxia. *Gene.* **354**, 157-161 (2005).

78. Marmolino D, Manto M, Acquaviva F, et al. PGC-1alpha down-regulation affects the antioxidant response in Friedreich's ataxia. *PLoS One*. **7**, 5–10025 (2010).
79. Marmolino D. Friedreich's ataxia: past, present, and future. *Brains Res Rev J* **2**, 311-330 (2011).
80. Martelli A, Wattenhofer-Donze M, Schmucker S, et al. Frataxin is essential for extramitochondrial Fe-S cluster proteins in mammalian tissues. *Hum. Mol. Genet.* **16**, 2651–2658 (2007).
81. Martelli A and Puccio H. Dysregulation of cellular iron metabolism in Friedreich ataxia: from primary iron-sulfur cluster deficit to mitochondria iron accumulation. *Front in Pharmacol.* **5**, 130 (2014).
82. McCabe DJ, Wood NW, Ryan F, et al. Intrafamilial phenotypic variability in Friedreich ataxia associated with a G130V mutation in the FRDA gene. *Arch Neurol.* **59**, 296–300 (2002).
83. McCormack ML, Guttman RP, Schumann M, et al. Frataxin point mutations in two patients with Friedreich's ataxia and unusual clinical features. *J Neurol Neurosurg Psychiatry.* **68**, 661–664 (2000).
84. Meier T and Buyse G. Idefenone: an emerging therapy for Friedreich ataxia. *J Neurol.* **256**, 25–30 (2009).
85. Michael S, Petrocine SV, Qian J, et al. Iron and iron-responsive proteins in the cardiomyopathy of Friedreich's ataxia. *Cerebellum.* **5**, 257–267 (2006).
86. Montermini L, Richter A, Morgan K, et al. Phenotypic variability in Friedreich ataxia: role of the associated GAA triplet repeat expansion. *Ann. Neurol.* **41**, 675–682 (1997).
87. Nair M, Adinolfi S, Pastore C, et al. Solution structure of the bacterial frataxin ortholog, CyaY: mapping the iron binding sites. *Structure.* **12**, 2037–2048 (2004).
88. Napoli E, Taroni F, Cortopassi G. Frataxin, iron-sulfur clusters, heme, ROS, and aging. *Antioxid. Redox Signal.* **8**, 506–516 (2006).
89. Nie G, Sheftel AD, Kim SF, et al. Overexpression of mitochondrial ferritin causes cytosolic iron depletion and changes cellular iron homeostasis. *Blood.* **105**, 2161–2167 (2005).

90. Parkinson MH, Boesch S, Nachbauer W, et al. Clinical features of Friedreich's ataxia: classical and atypical phenotypes. *J Neurochem.* **1**, 103–117 (2013).
91. Pastore A and Puccio H. Frataxin: a protein in search for a function. *J Neurochem.* **126**, 43–52 (2013).
92. Patel M, Isaacs C, Seyer L, et al. Progression of Friedreich ataxia: quantitative characterization over five years. *Ann Clin Transl Neurol.* **3**, 684–694 (2016).
93. Paupe V, Dassa E, Goncalves S, et al. Impaired nuclear Nrf2 translocation undermines the oxidative stress response in Friedreich ataxia. *PLoS One.* **4**, e4253 (2009).
94. Priller J, Scherzer C, Faber P, et al. Frataxin gene of Friedreich's ataxia is targeted to mitochondria. *Ann Neurol.* **42**, 265–269 (1997).
95. Prischi F, Konarev PV, Iannuzzi C, et al. Structural bases for the interaction of frataxin with the central components of iron-sulphur cluster assembly. *Nat Commun.* **1**, 95 (2010).
96. Puccio H, Simon D, Cossee M, et al. Mouse models for Friedreich ataxia exhibit cardiomyopathy, sensory nerve defect and Fe-S enzyme deficiency followed by intramitochondrial iron deposits. *Nat Genet.* **27**, 181–186 (2001).
97. Ramirez RL, Qian J, Santambrogio P, et al. Relation of cytosolic iron excess to cardiomyopathy of Friedreich's ataxia. *Am.J. Cardiol.* **110**, 1820–1827 (2012).
98. Richardson DR. Friedreich's ataxia: iron chelators that target the mitochondrion as a therapeutic strategy? *Expert Opin Invest Drugs.* **12**, 235–245 (2003).
99. Richardson DR, Lane DJ, Becker EM, et al. Mitochondrial iron trafficking and the integration of iron metabolism between the mitochondrion and cytosol. *Proc Natl Acad. Sci. USA* **107**, 10775–10782 (2010).
100. Riessland M, Brichta L, Hahnen E, et al. The benzamide M344, a novel histone deacetylase inhibitor, significantly increases SMN2 RNA/protein levels in spinal muscular atrophy cells. *Hum. Genet.* **120**, 101–110 (2006).

101. Ristow M, Pfister M, Yee A, et al. Frataxin activates mitochondrial energy conversion and oxidative phosphorylation *PNAS*. **97**, 12239-12243 (2000).
102. Rotig A, de Lonlay P, Chretien D, et al. Aconitase and mitochondrial iron-sulphur protein deficiency in Friedreich ataxia. *Nat. Genet.* **17**, 215–217 (1997).
103. Rouault T. Systemic iron metabolism: A review and implications for brain iron metabolism. *Pediatr Neurol.* **25**, 130–137 (2001).
104. Roy C and Andrews N. Recent advances in disorders of iron metabolism: Mutations, mechanisms and modifiers. *Hum Mol Genet.* **10**, 2181–2186 (2001).
105. Rustin P, von Kleist-Retzow JC, Chantrel-Groussard K, et al. Effect of idebenone on cardiomyopathy in Friedreich's ataxia: a preliminary study. *Lancet.* **354**, 477–479 (1999).
106. Saint-Georges Y, Garcia M, Delaveau T, et al. Yeast mitochondrial biogenesis: a role for the PUF RNA-binding protein Puf3p in mRNA localization. *PLoS One.* **3**, 2293 (2008).
107. Santos M, Ohshima K, Pandolfo M. Frataxin deficiency enhances apoptosis in cells differentiating into neuroectoderm. *Hum. Mol. Genet.* **10**, 1935–1944 (2001).
108. Santos R, Buisson N, Knight SA, et al. *Candida albicans* lacking the frataxin homologue: a relevant yeast model for studying the role of frataxin. *Mol. Microbiol.* **54**, 507–519 (2004).
109. Santos R, Lefevre S, Sliwa D, et al. Friedreich Ataxia: molecular mechanisms, redox considerations, and therapeutic opportunities. *Antioxid Redox Signal.* **13**, 651–690 (2010).
110. Schmucker S, Martelli A, Colin F, et al. Mammalian frataxin: an essential function for cellular viability through an interaction with a preformed ISCU/NFS1/ISD11 iron-sulfur assembly complex. *PLoS ONE.* **6**, e16199 (2011).
111. Schulz J, Dehmer T, Schöls L, et al. Oxidative stress in patients with Friedreich ataxia. *Neurology.* **55**, 1719–1721 (2000).
112. Seguin A, Bayot A, Dancis A, et al. Overexpression of the yeast frataxin homolog (Yfh1): contrasting effects on iron–sulfur cluster assembly, heme synthesis and resistance to oxidative stress. *Mitochondrion* **9**, 130–138 (2009).

113. Seznec H, Simon D, Monassier L, et al. Idebenone delays the onset of cardiac functional alteration without correction of Fe-S enzymes deficit in a mouse model for Friedreich ataxia. *Hum. Mol. Genet.* **13**, 1017–1024 (2004).
114. Sharma R, De Biase I, Gómez M, et al. Friedreich ataxia in carriers of unstable borderline GAA triplet-repeat alleles. *Ann. Neurol.* **56**, 898–901 (2004).
115. Sohn Y, Breuer W, Munnich A, et al. Redistribution of accumulated cell iron: a modality of chelation with therapeutic implications. *Blood.* **111**, 1690–1699 (2008).
116. Tsai C, Bridwell-Rabb J, Barondeau DP. Friedreich's ataxia variants I154F and W155R diminish frataxin-based activation of the iron-sulfur cluster assembly complex. *Biochemistry.* **50**, 6478–6487 (2011).
117. Vaubel RA and Isaya G. Iron-sulfur cluster synthesis, iron homeostasis and oxidative stress in Friedreich ataxia. *Mol. Cell. Neurosci.* **55**, 50–61 (2013).
118. Vazquez-Manrique RP, Gonzalez-Cabo P, Ros S, et al. Reduction of *Caenorhabditis elegans* frataxin increases sensitivity to oxidative stress, reduces lifespan, and causes lethality in a mitochondrial complex II mutant. *FASEB J.* **20**, 172–174 (2006).
119. Walden WE. From bacteria to mitochondria: aconitase yields surprises. *Proc. Natl. Acad. Sci. U.S.A.* **99**, 4138–4140 (2002).
120. Winterbourn CC and Hampton MB. Thiol chemistry and specificity in redox signaling. *Free Radic Biol Med.* **145**, 549–561 (2008).
121. Wilson RB, Lynch DR, Fischbeck KH. Normal serum iron and ferritin concentrations in patients with Friedreich's ataxia. *Ann Neurol.* **44**, 132-134 (1998).
122. Worth AJ, Basu SS, Deutsch EC, et al. Stable isotopes and LC-MS for monitoring metabolic disturbances in Friedreich's ataxia platelets. *Bioanalysis.* **7**, 1843-1855 (2015).
123. Yoon T and Cowan JA Iron-sulfur cluster biosynthesis. Characterization of frataxin as an iron donor for assembly of [2Fe-2S] clusters in ISU-type proteins. *J. Am. Chem. Soc.* **125**, 6078–6084 (2003).

124. Yoon T and Cowan JA. Frataxin-mediated iron delivery to ferrochelatase in the final step of heme biosynthesis. *J. Biol.Chem.* **279**, 25943–25946 (2004).
  
125. Zuhlke CH, Dalski A, Habeck M, et al. Extension of the mutation spectrum in Friedreich's ataxia: detection of an exon deletion and novel missense mutations. *Eur J Hum Genet.* **12**, 979–982 (2004).